PLOS | PATHOGENS

RESEARCH ARTICLE

ATPaseTb2, a Unique Membrane-bound FoF1-ATPase Component, Is Essential in Bloodstream and Dyskinetoplastic Trypanosomes

Karolína Šubrtová[1,2], Brian Panicucci[1], Alena Zíková[1,2]*

1 Institute of Parasitology, Biology Centre, CAS, České Budějovice, Czech Republic, **2** Faculty of Science, University of South Bohemia, České Budějovice, Czech Republic

* azikova@paru.cas.cz

CrossMark
click for updates

OPEN ACCESS

Citation: Šubrtová K, Panicucci B, Zíková A (2015) ATPaseTb2, a Unique Membrane-bound FoF1-ATPase Component, Is Essential in Bloodstream and Dyskinetoplastic Trypanosomes. PLoS Pathog 10(2): e1004660. doi:10.1371/journal.ppat.1004660

Editor: Achim Schnaufer, University of Edinburgh, UNITED KINGDOM

Received: June 13, 2014

Accepted: January 6, 2015

Published: February 25, 2015

Copyright: © 2015 Šubrtová et al. This is an open access article distributed under the terms of the Creative Commons Attribution License, which permits unrestricted use, distribution, and reproduction in any medium, provided the original author and source are credited.

Data Availability Statement: All relevant data are within the paper and its Supporting Information file.

Funding: This work was funded by Ministry of Education ERC CZ grant LL1205, the Czech Grant Agency grant P302/12/2513, the EMBO Installation grant 1965 (to AZ) and the Grant Agency of University of South Bohemia grants 140/2010/P and 04/092/2011/P (to KS). We acknowledge the use of research infrastructure that has received funding from the European Union Seventh Framework Programme (FP7/2007-2013) under grant agreement no.316304. The funders had no role in study design, data

Abstract

In the infectious stage of *Trypanosoma brucei*, an important parasite of humans and livestock, the mitochondrial (mt) membrane potential ($\Delta\psi_m$) is uniquely maintained by the ATP hydrolytic activity and subsequent proton pumping of the essential F_oF_1-ATPase. Intriguingly, this multiprotein complex contains several trypanosome-specific subunits of unknown function. Here, we demonstrate that one of the largest novel subunits, ATPaseTb2, is membrane-bound and localizes with monomeric and multimeric assemblies of the FoF1-ATPase. Moreover, RNAi silencing of ATPaseTb2 quickly leads to a significant decrease of the $\Delta\psi_m$ that manifests as a decreased growth phenotype, indicating that the F_oF_1-ATPase is impaired. To further explore the function of this protein, we employed a trypanosoma strain that lacks mtDNA (dyskinetoplastic, Dk) and thus subunit a, an essential component of the proton pore in the membrane F_o-moiety. These Dk cells generate the $\Delta\psi_m$ by combining the hydrolytic activity of the matrix-facing F_1-ATPase and the electrogenic exchange of ATP^{4}- for ADP^{3}- by the ATP/ADP carrier (AAC). Surprisingly, in addition to the expected presence of F1-ATPase, the monomeric and multimeric F_oF_1-ATPase complexes were identified. In fact, the immunoprecipitation of a F_1-ATPase subunit demonstrated that ATPaseTb2 was a component of these complexes. Furthermore, RNAi studies established that the membrane-bound ATPaseTb2 subunit is essential for maintaining normal growth and the $\Delta\psi_m$ of Dk cells. Thus, even in the absence of subunit a, a portion of the F_oF_1-ATPase is assembled in Dk cells.

Author Summary

The presence of the F_oF_1-ATP synthase in every aerobic organism suggests that evolution has settled on a basic blueprint for the complex rotary motor capable of synthesizing life's universal energy currency—ATP. However, compared to yeast and mammalian models of the F_oF_1-ATP synthase, several recent studies have reported unique structural and functional features of this complex from organisms representing the clades of Chromalveolata,

collection and analysis, decision to publish, or preparation of the manuscript.

Competing Interests: The authors have declared that no competing interests exist.

Archaeplastida and Excavata. One of the most striking cases is observed in trypanosomes, important parasites of humans and animals. Notably, the F_oF_1-ATP synthase/ATPase switches from synthesizing ATP in the insect vector life stage to hydrolyzing ATP in their mammalian hosts to generate the essential mitochondrial membrane potential ($\Delta\psi_m$). Moreover, this indispensable F_oF_1-ATPase contains up to 14 trypanosome-specific subunits. Here we characterize one such novel subunit, ATPaseTb2. We demonstrate that this subunit is crucial for the survival of the infectious stage of trypanosomes, part of the fully assembled F_oF_1-complex and it is essential for maintaining the $\Delta\psi_m$. Given the enzyme's irreplaceable function and extraordinary composition, we believe that the F_oF_1-ATPase is an attractive drug target.

Introduction

Trypanosomes are unicellular flagellates from the order Kinetoplastida, which is comprised of some of the most devastating human pathogens in the world. For example, in sub-Saharan Africa, infection from *Trypanosoma brucei gambiense* and *T. b. rhodesiense* causes Human African Trypanosomiasis, which is almost always fatal if left untreated [1]. The latest WHO reports estimate that there are 10,000 new cases annually in endemic regions. Meanwhile, a third subspecies, *T. b. brucei*, infects livestock and therefore negatively affects the human population through malnutrition and economic hardships [2,3].

T. brucei parasites have a complex life cycle, alternating between the mammalian host and the insect vector, a tse-tse fly. During this environmental switch, the protist undergoes rapid and dramatic changes in cell morphology and metabolism [4–6]. In particular, the single mitochondrion undergoes extensive remodelling, which reflects the adaptability of the parasite to consume different carbon sources based on their availability [4]. The procyclic (insect) form (PF) of trypanosomes catabolizes amino acids and maintains a well-developed mitochondrion with abundant cristae, Krebs cycle enzymes and a complete oxidative phosphorylation pathway. This pathway includes enzymatic complexes that generate a mitochondrial (mt) membrane potential ($\Delta\psi_m$) that is coupled to ATP synthesis by the F_oF_1-ATP synthase [5]. In contrast, the bloodstream form (BF) of this parasite populates the glucose-rich fluids (e.g. blood and spinal fluid) of its vertebrate host, allowing them to utilize just glycolysis for ATP production. This results in a drastically reduced mitochondrion that lacks significant cristae, key enzymes of the Krebs cycle and the cytochrome-containing respiratory complexes that pump protons into the inner mt membrane space [6,7]. Despite this reduction, the BF mitochondrion is still an active organelle, holding vital processes e.g. lipid metabolism [8], ion homeostasis [9], calcium signalling [10,11], FeS cluster assembly [12] and acetate production for *de novo* lipid biosynthesis [13]. Importantly, in the absence of proton-pumping respiratory complexes III and IV, the indispensable $\Delta\psi_m$ is sustained mainly by the hydrolytic activity of the F_oF_1-ATPase. Thus, this complex possesses an essential, unique and irreplaceable function in BF mitochondria [14].

In other eukaryotes, this reverse activity of the F_oF_1-ATP synthase is observed only rarely, for very brief moments of time and under very specific conditions (i.e. during oxygen deprivation or in response to damaged or mutated mt respiratory proteins). When the function of the respiratory complexes is compromised, the $\Delta\psi_m$ falls below a physiological threshold and is restored by the reverse proton pumping activity of the F_oF_1-ATPase, which is powered by ATP hydrolysis. The hydrolytic activity of the catalytic F_1-ATPase is also essential for exceptional cells that lack mtDNA (ρ° cells). These cells do not express several core subunits of the

membrane embedded F_o-moiety (subunits 6, 8 and 9 in yeast, subunits a and A6L in bovine) of the F_oF_1-ATPase, notably those that are components of the proton pore. Thus, the matrix protruding F_1-ATPase energizes the inner mt membrane by coupling ATP hydrolysis with the exchange of ADP^{3-} for ATP^{4-} by the ATP/ADP carrier (AAC) [15]. The same mechanism for producing the $\Delta\psi_m$ is utilized by trypanosomes that lack a mt genome, which is called a kinetoplast [16]. These naturally occuring dyskinetoplastic forms (Dk) of *T. brucei* (e.g. *T. b. evansi* or *T. b.equiperdum*) cause economically significant diseases in horses, camels, and water buffaloes. Remarkably, these parasites are not able to switch to the insect stage and are transmitted mechanically by bloodsucking insects or by coitus [17]. The mtDNA-lacking trypanosomes can also be chemically induced in the laboratory (e.g. Dk *T. brucei* EATRO164) [18]. Interestingly, each of the Dk cell lines characterized so far, bear one of several different compensatory mutations in the nuclear encoded subunit γ that enable the $\Delta\psi_m$ to be generated independently of the F_o-moiety [14,16,19].

In general, the F_oF_1-ATP synthase complex consists of two functionally distinct enzymatic segments: the hydrophilic F_1 catalytic moiety and the membrane-bound F_o pore. Both of these subcomplexes are linked together by the central and peripheral stalks. The central stalk rotates with the c-ring when protons are allowed to pass through the F_o pore, located between the c-ring and subunit a. In contrast to the rotation of the central stalk, the stationary peripheral stalk plays a crucial role in keeping the catalytic F_1 headpiece static, thus resisting the rotational torque. The eubacterial F_1-moiety consists of the catalytic domain and the central stalk, which are comprised of five subunits in a stoichiometry of α_3, β_3, γ_1, δ_1, ε_1. The F_o-moiety is composed of the oligomeric c_{10-15} ring and a single subunit a joined together with two copies of subunit b, which extend from the membrane and form the base of the peripheral stalk. The composition of the eukaryotic enzyme has been determined mainly from detailed studies of F_oF_1-ATP synthase purified from the mitochondria of *Bos taurus* and *Saccharomyces cerevisiae*, members of the clade Opisthokonta. These enzymes contain homologous prokaryotic-like core components, but also incorporate additional eukaryotic specific subunits involved in the structure, oligomerization and regulation of the complex [20]. These novel subunits have been assigned to various regions of the F_oF_1-ATP synthase: i) subunit ε and inhibitory factor 1 (IF_1) bind to the F_1-moiety; ii) the small hydrophobic subunit 8 (subunit A6L in bovine) is located in the membrane interacting with subunit a; iii) the soluble subunit h (subunit F_6 in bovine), oligomycin sensitivity-conferring protein (OSCP) and hydrophilic subunit d are assigned to the peripheral stalk; iv) subunits e, f, g, all containing one transmembrane helix, are regarded as accessory peripheral stalk proteins that predominantly reside in the inner membrane where they presumably stabilize the utmost hydrophobic subunit 6 (or subunit a in bovine), thereby assisting the peripheral stalk with its stator function [21–23].

Recently, however, several studies have reported unique structural and functional features of the F_oF_1-ATP synthase from medically relevant parasites and other organisms that represent the clades of Chromalveolata [24], Archaeplastida [25] and Excavata [26]. In *Plasmodium falciparum*, a member of the phylum Apicomplexa, the genomic data indicates the likely presence of all eukaryotic F_1 subunits and some of the F_o and stator subunits [27]. Conspicuously absent are the subunits a and b, which are crucial to the function of all known F_oF_1-ATP synthases. These subunits are also missing in the ATP synthase of *P. yoelii* and *Tetrahymena thermophila*, the latter a member of the sister phylum Ciliophora, both of which have been shown experimentally to possess ATP synthase activity [28–30]. This suggest that ciliates and apicomplexan species employ highly divergent or novel subunits to fulfil the functions of the classical subunits a and b. Another example of an unusual F_oF_1-ATP synthase complex comes from studies of the chlorophycean algea *Chlamydomonas reinhardtii* and *Polytomella* sp. that determined the

complex contains up to 9 unique subunits (Asa1-Asa9) that either form an innovative peripheral stator or are responsible for complex dimerization [31].

Trypanosoma F_oF_1-ATP synthase consists of the well conserved F_1-moiety comprised of subunits α, β, γ, δ, ε and the trypanosome-specific subunit p18 [26,32], and the less characterized F_o pore and peripheral stalk where only subunits c, a and OSCP were identified at the gene or protein level [26,33]. Additionally, the complex contains up to 14 Kinetoplastida-specific subunits that lack homology to any of the previously described subunits. Therefore, their position within the complex and their function is unknown. Interestingly, these recently identified F_oF_1-ATP synthase subunits specific for *T. brucei* (ATPaseTb) may represent early evolutionary attempts to create the functional and structural components of the eukaryotic accessory subunits for this early divergent species. Previously, two of these novel subunits, ATPaseTb1 (Tb10.70.7760) and ATPaseTb2 (Tb927.5.2930), were shown to be essential for the proper function and structural integrity of F_oF_1-ATP synthase in the procyclic form of this parasite [26].

Here, we have extended this study and functionally characterized ATPaseTb2 in the disease-relevant stage of *T. brucei* and Dk *T. b evansi*. Our results demonstrate that the membrane-bound ATPaseTb2 protein is indispensable for the survival of BF and Dk trypanosomes because it is crucial for maintaining the $\Delta\psi_m$ in these cells. Furthermore, the unexpected observation of assembled F_oF_1-ATPase complexes in two different strains of trypanosomes lacking mt DNA suggests that the composition of the Dk F_oF_1-ATPase complex is more similar to the BF F_oF_1-ATPase complex than previously thought.

Results

Bioinformatics reveals that ATPaseTb2 contains a putative transmembrane domain and a region homologous to the bovine subunit d

ATPaseTb2 is annotated as a hypothetical protein in the TriTrypDB database (www.tritrypdb.org) and its mt localization was predicted by the presence of an N-terminal mt targeting sequence assigned by Mitoprot II v1.101 [34] (probability 0.823). Strikingly, this subunit has no detectable homologs outside Kinetoplastida based on a similarity sequence search (e.g. BLAST). To uncover any homologous relationships for protein sequences that do not share high enough sequence identity, but might have similar secondary structure, we employed the HHpred toolkit (http://toolkit.tuebingen.mpg.de), which is based on an HMM-HMM comparison that reveals homologous relationships even if the sequences share less than 20% sequence identity [35]. All of the available Kinetoplastida ATPaseTb2 homologs obtained from the TriTrypDB (S1A Fig.) were analyzed using HHpred software. Among the first five structural homologs detected was the bovine F_oF_1-ATP synthase subunit d, with a probability of 44.7 and a P-value of 0.0021. Then a consensus sequence generated from an alignment of this 92 amino acids (aa) region from all identified kinetoplastida homologs was resubmitted for HHpred analysis. This search returned a significant hit to the bovine subunit d with a probability of 78.1 and a P-value of 0.0002 (S1B Fig.). This bovine F_oF_1-ATP synthase subunit is comprised of 160 aa and resides within the peripheral stalk where it interacts with all the other three components of the peripheral stalk (b, F_6 and OSCP). This subunit is predominantly hydrophilic, contains several long alpha-helices and is essential for the enzymatic function [23,36,37]. The region of similarity to subunit d falls in the middle of the ATPaseTb2 sequence and it is followed by a putative trans-membrane (TM) domain (aa 239–254) that was predicted by MEMSAT-SVM software (http://bioinf.cs.ucl.ac.uk/psipred/) [38] with a -0.738 prediction score (Fig. 1). This prediction is intriguing because a typical eukaryotic subunit d is not directly attached to the

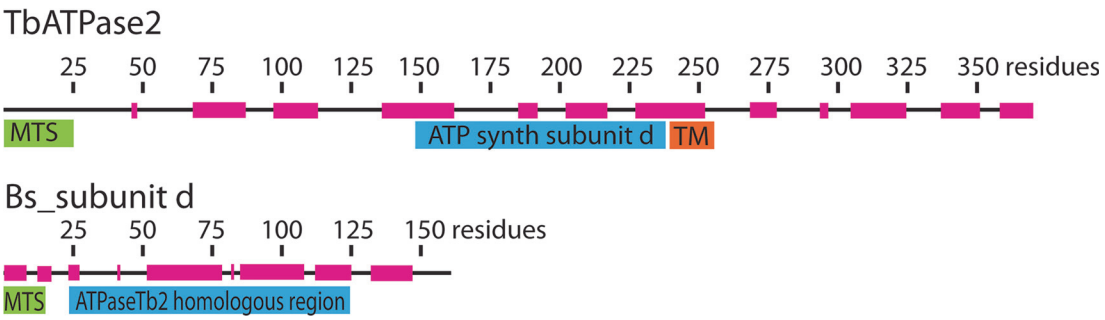

Fig 1. Bioinformatics reveal that ATPaseTb2 possesses a region of low homology to ATPase subunit d. A schematic representation depicting the ATPaseTb2 protein (370 aminoacids (AA)) and the *Bos taurus* subunit d (Bs_sub d, 161 AA) was created using Adobe Illustrator CS5.1. The mitochondrial targeting signals (MTS, green) were predicted by Mitoprot II v1.101. The transmembrane domain (TM, orange) within the ATPaseTb2 sequence was predicted by MEMSAT-SVM software. The homologous region (blue) to Bs_sub d was determined using HHpred toolkit. The regions of alpha-helices (magenta) depicted on the amino acid sequence line were predicted by software from EMBOSS garnier.

doi:10.1371/journal.ppat.1004660.g001

membrane, but rather it interacts with the soluble region of the membrane-bound subunit b via three coiled-coil interactions [23]. Thus, ATPaseTb2 may represent a novel subunit of the membrane-bound peripheral stalk that possibly depicts an early divergent functional alternative of the stator by creating a chimera of subunits b and d.

ATPaseTb2 is a mt membrane-bound protein expressed in various forms of *T. brucei*

The mitochondrial localization, as well as the structural and functional association of ATPaseTb2 with the F_oF_1-ATP synthase in PF *T. brucei* cells was previously described [26]. Because the activity of this complex significantly differs between the insect and mammalian stage of the parasite, we were interested if the ATPaseTb2 protein is also expressed in trypanosomes residing in the bloodstream of their host. Therefore, we cultured PF427 (insect stage), BF427 (bloodstream forms) and the laboratory-induced dyskinetoplastic Dk164 *T. brucei* cells, in addition to the naturally occurring Dk *T.b.evansi*. Whole cell lysates from PF427, BF427, Dk164 and *T. b.evansi* cells were fractionated by SDS-PAGE and analyzed by western blot using a specific polyclonal antibody against ATPaseTb2 (Fig. 2A). Interestingly, ATPaseTb2 is expressed in all four cell types; however, its expression is significantly decreased in BF427 and even more reduced in Dk164 and *T.b.evansi* cells. A similar expression pattern for F_1-ATPase subunit β and mt chaperone Hsp70 was also observed between PF, BF and Dk cells (Fig. 2A). These results are in agreement with the proposed reduction of the mitochondria size, function and activity in the various bloodstream forms of *T. brucei* [39].

To experimentally investigate the subcellular localization of ATPaseTb2 within the bloodstream *T. brucei* cell, the ATPaseTb2 gene product was C-terminally tagged with a v5-tag and inducibly expressed using tetracycline (tet). Cytosolic and mitochondrial fractions were isolated from a hypotonic lysate of cells over-expressing the ATPaseTb2_v5 protein. The mitochondrial fractions were then treated with digitonin to create mitoplasts that were further incubated with sodium carbonate (Na_2CO_3) to obtain mt membrane and mt matrix fractions. The subsequent western analyses established the purity of the extracted fractions as the cytosolic enolase, the mt inner membrane carrier protein (AAC) and the matrix-localized guide RNA binding protein (MRP1) were confined within their respective subcellular fractions. Notably, ATPaseTb2 was predominantly localized in the mt membrane fraction, while subunit β of the matrix-soluble F_1-ATPase was released into the matrix fraction (Fig. 2B), demonstrating that ATPaseTb2 is firmly embedded in the inner mt membrane.

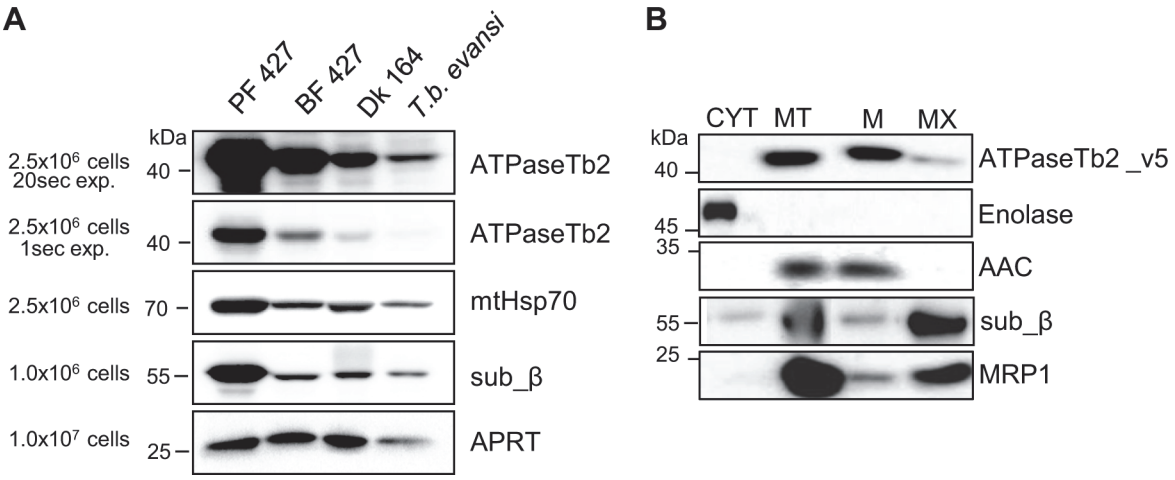

Fig 2. ATPaseTb2 is expressed in PF427, BF427, Dk164 *T. brucei* and *T. b. evansi* cells and it is a membrane-bound protein. A) The steady state abundance of ATPaseTb2 (two different exposure times), subunit β, mtHsp70 and cytosolic adenosine phosphoribosyl transferase (APRT) was determined in PF427, BF427, Dk164 and *T. b. evansi* cells by western blot analysis of whole cell lysates from $2.5x10^6$ cells or $1x10^6$ cells (for subunit β and APRT) resolved on SDS-PAGE gels. The pertinent sizes of the protein marker are indicated on the left. B) Subcellular localization of ATPaseTb2 was determined using BF cells expressing v5-tagged ATPaseTb2. Cytosolic (CYT) and mitochondrial (MT) fractions were obtained by hypotonic lysis. Mt pellets were further treated with Na_2CO_3 and spun at a high-speed to obtain mt membrane (M) and matrix (MX) fractions. Purified fractions were analyzed by western blot with the following antibodies: anti-v5 (ATPaseTb2_v5), anti-enolase (cytosol), anti-AAC (mt inner membrane), anti-β (F_1-ATPase subunit) and anti-MRP1 (mt matrix). The relevant sizes of the protein marker are indicated on the left.

doi:10.1371/journal.ppat.1004660.g002

ATPaseTb2 is a bona fide subunit of F_oF_1-ATPase monomers and higher oligomers

To confirm that ATPaseTb2 is a genuine subunit of both the BF and Dk F_oF_1-ATPase, we employed the same strategy applied previously for PF cells [26]. Therefore, we first created BF cell lines in which either the ATPaseTb2 or the F_1 subunit p18 were inducibly expressed with a C-terminal tag. Complexes assembled with a tagged protein were then purified using a one-step IgG affinity purification, followed by treatment with TEV protease to release bound complexes from the IgG beads. The TEV eluates were further analyzed by western blot for the presence of the tagged proteins, known F_oF_1-ATPase subunits, and AAC (Fig. 3A). Importantly, the presence of the tagged subunits ATPase Tb2 and p18 in the respective cell lines were confirmed using a specific antibody against the *c*-myc epitope that comprises part of the tag. In addition, the ATPaseTb2_TAP eluate contained F_oF_1-ATPase subunits β, p18 and ATPaseTb1. Vice versa, the p18_TAP eluate contained subunits ATPaseTb2, ATPaseTb1 and subunit β. While AAC has been described to associate with mammalian F_oF_1-ATPase under certain conditions [40], it is not a core component of the enzyme and the lack of its signal indicates the stringency of this technique. The TAP tag purification from non-induced cells was used as a negative control to verify that the detected proteins do not bind non-specifically to the charged beads. To analyze the composition of the Dk F_oF_1-ATPase, p18 tagged complexes were purified and subjected to the same set of antibodies described for the BF complexes (Fig. 3B). These results also depicted the same interactions seen in Fig. 3A. Therefore, the co-purification of ATPaseTb2 with known ATPase subunits p18 and β validates that it is an authentic constituent of the F_oF_1-ATPase complex in both BF and Dk cells.

The sedimentation profile of F_oF_1-ATP synthase in 10–30% glycerol gradients (GG) was previously published and revealed two distinct regions representing the F_1-moiety and the F_oF_1-monomer and multimeric complexes [26]. In order to specify if ATPaseTb2 is a component of the F_1-moiety or the F_oF_1-complex, the glycerol gradient sedimentation profile was

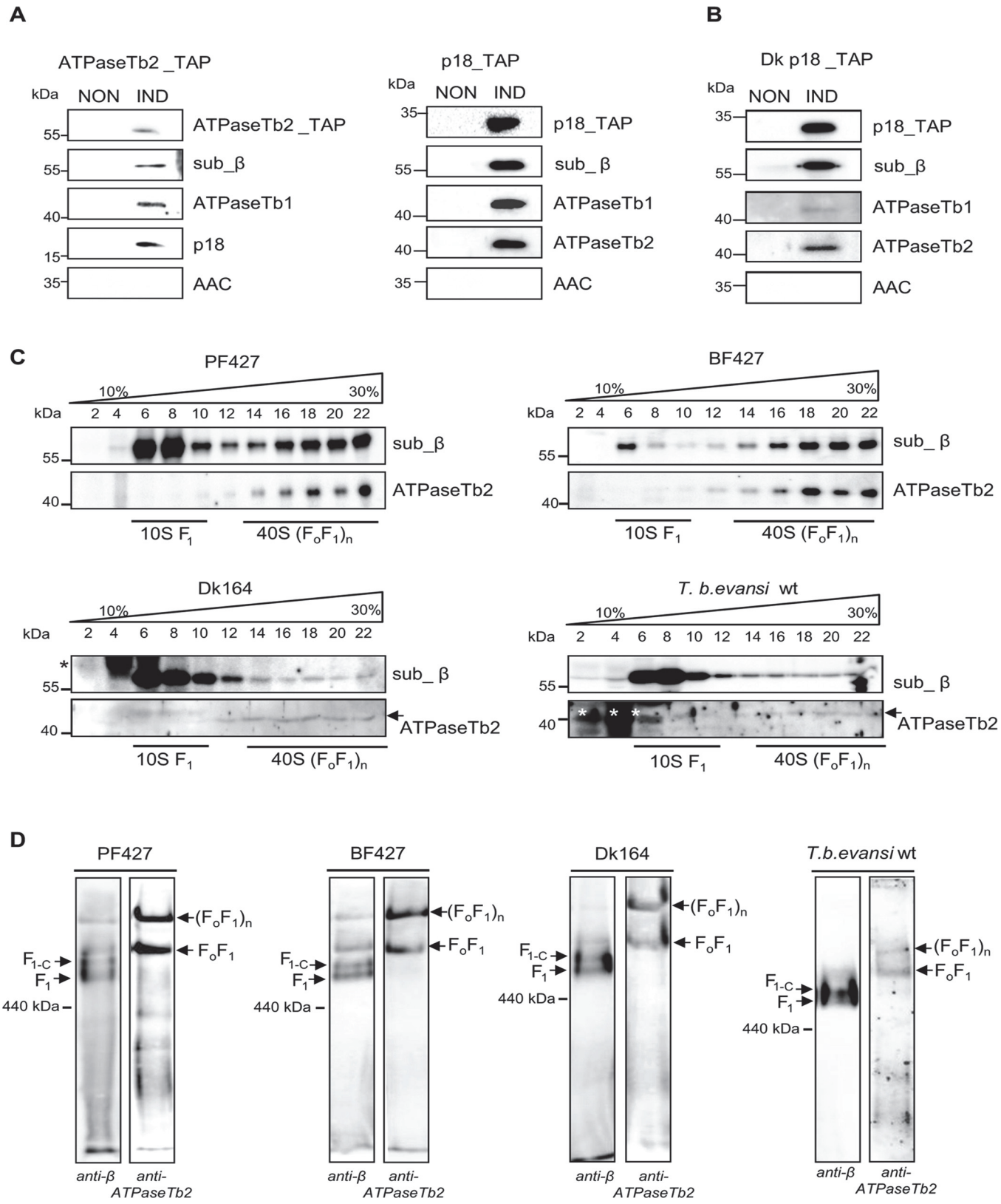

Fig 3. ATPaseTb2 is a bona fide subunit of the monomeric and multimeric F_oF_1-ATPases. A) ATPaseTb2_TAP and p18_TAP tagged complexes were purified from BF cells using one-step IgG affinity chromatography from non-induced (NON) and 2 days induced (IND) cells containing the regulatable ectopic

TAP tagged protein. The tagged protein complexes were eluated by TEV protease, fractionated on SDS-PAGE and examined by western blot analyzes. The presence of the tagged ATPaseTb2 and p18 subunits was verified using a *c*-myc antibody (top panels: ATPaseTb2_TAP and p18_TAP). The known F_oF_1-ATPase subunits (sub β, p18 and ATPase_Tb1) were detected using specific antibodies. The lack of signal for AAC serves as a control for specificity of the used method. The applicable sizes of the protein marker are indicated on the left. B) p18_TAP tagged complexes were purified from dyskinetoplastic *T. b. evansi* as described above for BF cells and subjected to the same set of antibodies. C) The sedimentation profile of F_1- and F_oF_1-ATPase complexes was determined using glycerol gradient sedimentation. Hypotonically purified mitochondria from PF427, BF427, Dk164 and *T. b. evansi* cells were lysed with 1% Triton X-100 and fractionated on a 10–30% glycerol gradient. The glycerol gradient fractions were collected, fractionated by SDS-PAGE and analyzed by western blots. Western analyzes with an anti-β antibody depicted the sedimentation profile of the F_1-ATPase and monomeric/multimeric F_oF_1-ATP synthase complexes, whereas the anti- ATPaseTb2 antibody only immunodecorates this protein within the monomeric/multimeric F_oF_1-ATPase complexes. The subdivision of the various structural forms of the F_oF_1-ATPase complexes are underlined as determined in [26]. The glycerol gradient fractions and the sizes of the protein marker are indicated. Nonspecific bands visible in Dk164 and *T. b. evansi* gradients are indicated by asterisks. D) The native F_1- and F_oF_1-ATPase complexes were visualized using hrCNE. Purified mitochondria from PF427, BF427, Dk164 and *T.b.evansi* cells were lysed with digitonin (4 mg/mg), fractionated on a 3%-12% hrCNE and blotted onto a nitrocellulose membrane. The F_1-ATPase (F_1), the F_1-ATPase bound with the c-ring (F_{1+C}) and the monomeric F_oF_1/multimeric $(F_oF_1)_n$ complexes were all visualized using specific polyclonal antibodies against either subunit β or ATPaseTb2. The size of ferritin from the equine spleen (440 kDa) is indicated on the left.

doi:10.1371/journal.ppat.1004660.g003

determined using mt lysates from all four cell types: PF427, BF427, Dk164 and *T.b.evansi*. In correlation with the literature, a new specific antibody raised against the F_1-subunit β depicted both regions, which are defined as ∼10S (fractions 6–10), and ∼40S (fractions 14–22) (Fig. 3C). A different sedimentation pattern was revealed when a specific antibody recognizing ATPaseTb2 detected only the 40S region (fractions 14–22), representing the F_oF_1-monomer and -multimers. These findings suggest that the novel subunit is not a component of the F_1-moiety, but rather a member of the fully assembled complex. Furthermore, compelling results hinting at the function of this hypothetical protein were also obtained when the mt lysates of Dk164 and *T. b. evansi* cells were fractionated on similar gradients. While the majority of the signal for subunit β was predictably detected in fractions 6–10, representing the F_1-ATPase complex, there was also a weak signal detected in higher S values. These same ∼40S complexes were identified using the ATPaseTb2 antibody (Fig. 3C). This indicates that in the absence of subunit a, the F_1-moiety is still attached to the mt membrane via a central stalk, a ring of subunit c and the peripheral stalk. Since the F_o subunit a is missing in these cells, the attachment of this complex to the membrane is presumably not as strong as in BF cells. Therefore, upon treatment with detergent to lyse the mitochondria, a majority of F_1-ATPase is released and detected in lower S values while a small portion of the F_oF_1-complexes is preserved and sediments at higher S value fractions. Consequently, our data suggests that previously undetected membrane-bound F_oF_1-complexes are present in the mitochondria of the Dk trypanosomes.

To verify our intriguing results, the F_oF_1-ATP synthase/ATPase complex was examined by an alternative method involving high resolution clear native electrophoresis (hrCNE) followed by western blot analysis. Results obtained using the antibody against subunit β revealed four predominant bands in both the PF427 and BF427 samples, representing various forms of the F_1-moiety and F_oF_1-complexes (Fig. 3D). The lowest band likely corresponds to the F_1-ATPase (subunits α, β, γ,δ,ε), while the one above it seemingly represents F_1-ATPase with a ring of subunit c, as it has been described for the mammalian complex [41]. Noticeably, in each sample the antibody against ATPaseTb2 immunodetected only two major bands corresponding to the F_oF_1-monomer and -multimers. When the mt lysates of Dk164 and *T. b. evansi* cells were fractionated on a hrCNE, subunit β was mainly detected in the lower bands representing the F_1-moiety and the F_oF_1-monomer, while only a weaker band was observed at the size depicting F_oF_1-multimers. But western blot analysis with the ATPaseTb2 antibody clearly demonstrated the existence of higher assemblies of the F_oF_1-ATPase complexes (Fig. 3D). Thus, ATPaseTb2 is a membrane-bound subunit of the monomeric and multimeric F_oF_1-ATP synthase/ATPase complex in all four *T. brucei* cell types examined. Furthermore, no significant differences in size were observed between the F_oF_1-monomeric and -multimeric complexes detected in

PF427, BF427 and Dk cells, indicating that subunit a might be the only missing component of the assembled F_oF_1-ATPase complex in dyskinetoplastic cells.

Silencing of ATPaseTb2 inhibits cell growth by decreasing the $\Delta\psi_m$ in BF *T. brucei*

To assess the importance of ATPaseTb2 in the infective stage of *T. brucei* and to evaluate its functional association with F_oF_1-ATPase, an ATPaseTb2 RNA interference (RNAi) cell line was created. The expression of dsRNA was triggered by the addition of tet to the culture medium and the *in vitro* growth of the ATPaseTb2 knock-down (KD) cells was inspected for seven days (Fig. 4A). Strikingly, a significant growth phenotype was already detected in RNAi induced cells on just the second day of tet addition. Presumably, the powerful selection forces acting on these cells missing a critical protein resulted in the emergence of a subpopulation that was no longer responsive to RNAi induction after only 120 hours, leading to the growth recovery of the culture (Fig. 4A). This phenomenon is often reported for RNAi experiments in BF *T. brucei* [42].

The targeted KD of ATPaseTb2 was confirmed by western blot analysis of whole cell lysates harvested from an equivalent number of cells for ATPaseTb2 RNAi non-induced and induced cells throughout the RNAi time course (Fig. 4B). Western blot analysis using the antibody against ATPaseTb2 exhibited a reduction of the targeted protein by 73% at day 2 of RNAi induction. A non-specific band detected on the same membrane was used to determine equal loading of the samples.

With the efficient knockdown of ATPaseTb2 verified, an *in vivo* assay was employed to measure the $\Delta\psi_m$ in the ATPaseTb2 KD cell population (Fig. 4C), since the $\Delta\psi_m$ is generated by the F_oF_1-ATPase in BF *T. brucei* [9]. Flow cytometry analysis was used to determine the changes observed in these cells stained with Mitotracker Red CMX-Ros, whose fluorescent intensity is proportionally dependent on the strength of the $\Delta\psi_m$. A substantial decrease of the $\Delta\psi_m$ in the KD cell population was observed two days (IND2) after RNAi induction, coinciding with the first time point to display a significant growth inhibition. Importantly, this result confirms the vital function of ATPaseTb2 within the F_oF_1-ATPase.

Depleting ATPaseTb2 does not significantly alter ATP hydrolysis capabilities

To assess if the decrease in the $\Delta\psi_m$ is the result of an impaired ATP hydrolytic activity of the enzyme, the total ATPase activity was measured in mt lysates with or without azide, an inhibitor of the catalytic F_1-ATPase [43]. Typically, the specific F_1-ATPase activity represents $\sim$ 35–45% of total mt ATPase activity. Our results indicate that neither the total ATPase nor azide-sensitive activities were significantly altered between the non-induced and ATPaseTb2 RNAi-induced cells (Fig. 5A). ATPase activity can also be visualized by in-gel activity staining when mitochondria from these cells are solubilized with dodecyl maltoside and separated on a 2–12% blue native PAGE (BNE) [41]. The specific ATPase staining revealed two major bands in non-induced cells, the predominant lower one representing the activity produced from the F_1-moiety and the less significant higher band representing the hydrolytic activity of the monomeric F_oF_1-ATPase (Fig. 5B). It is important to note that solubilizing mitochondria with any detergent can result in unintended structural consequences not found under normal physiological conditions, especially for a large complex comprised of a matrix moiety and a membrane embedded region. Although detergents tend to dissociate the F_1-moiety from F_oF_1-ATPase complexes, it is intriguing that there is still a portion of ATP hydrolysis being produced from

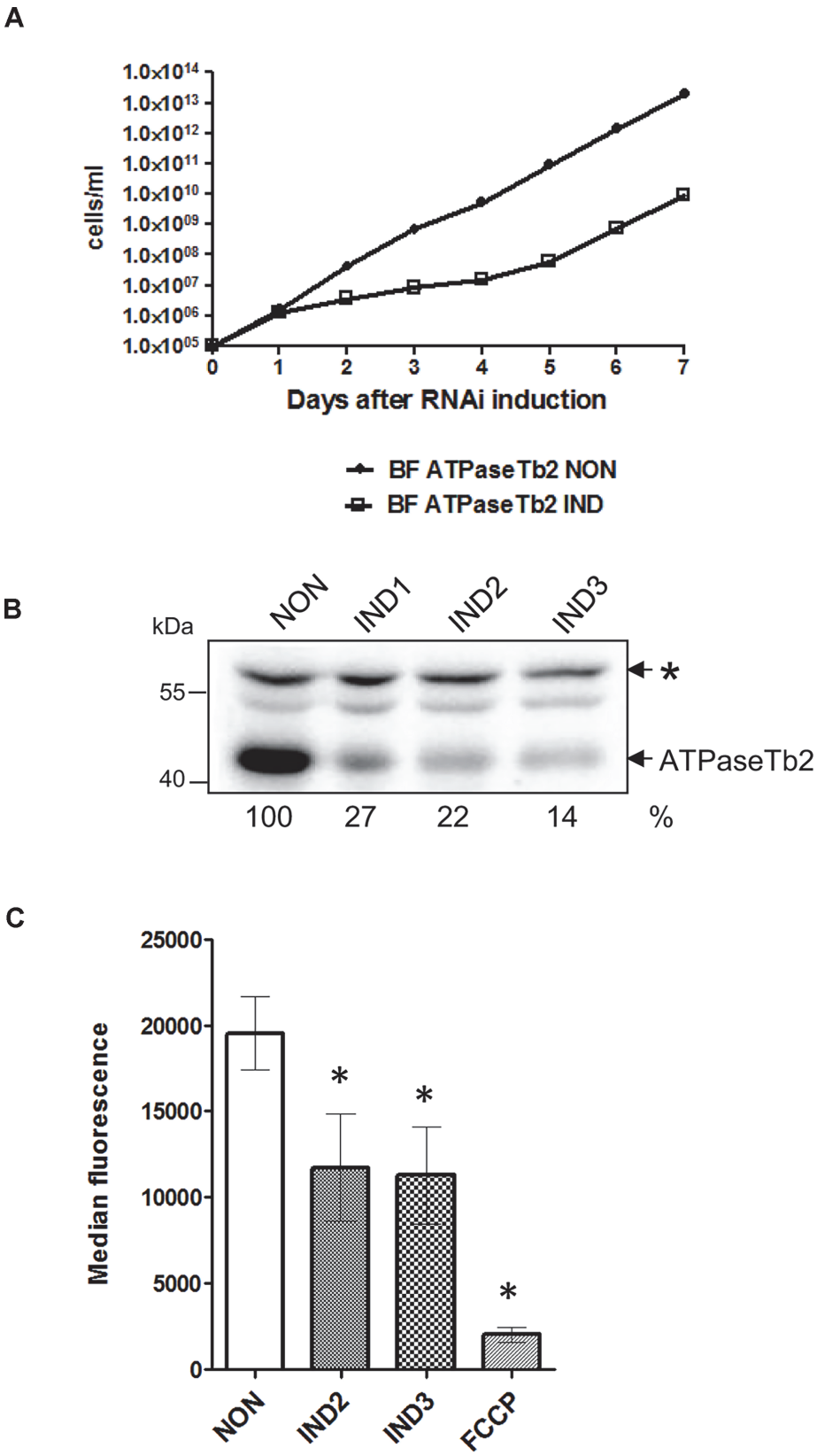
A
1.0x10^14
1.0x10^13
1.0x10^12
1.0x10^11
1.0x10^10
1.0x10^09
1.0x10^08
1.0x10^07
1.0x10^06
1.0x10^05
cells/ml
0
1
2
3
4
5
6
7
Days after RNAi induction
BF ATPaseTb2 NON
BF ATPaseTb2 IND
B
kDa
NON
IND1
IND2
IND3
55
40
*
ATPaseTb2
100
27
22
14
%
C
25000
20000
15000
10000
5000
0
Median fluorescence
*
*
*
NON
IND2
IND3
FCCP

Fig 4. RNAi silencing of ATPaseTb2 inhibits the growth and mt membrane potential of BF *T. brucei*. A) Growth curves of the noninduced (NON) and RNAi induced (IND) ATPaseTb2 RNAi bloodstream *T. brucei* cell lines were measured for 7 days. Cells were maintained in the exponential growth phase (between 10^5 and 10^6 cells/ml) and the cumulative cell number was calculated from cell densities adjusted by the dilution factor needed to seed the cultures at 10^5 cells/ml each day. The figure is representative of three independent RNAi-inductions. B) The steady-state abundance of ATPaseTb2 in non-induced (NON) RNAi cells and in cells induced with tet for 1, 2 and 3 days (IND1, IND2, IND3) was determined by western blot analysis using a specific ATPaseTb2 antibody. The non-specific band (marked with an asterisk) detected on the same membrane served as a loading control. The numbers beneath the blots represent the abundance of immunodetected ATPaseTb2 expressed as a percentage of the non-induced samples after normalizing to the loading control. The relevant sizes of the protein marker are indicated on the left. The figure is a representative western blot from three independent RNAi-inductions. C) Using Mitotracker Red CMX-Ros, the mt membrane potential was measured by flow cytometry in non-induced (NON) ATPaseTb2 RNAi cells and cells induced for 2 or 3 days (IND2 and IND3). The median fluorescence for each sample is depicted on the y-axis of the column graph. The results are means ± s.d. (n = 3). *$P < 0.05$, Student's *t*-test.

doi:10.1371/journal.ppat.1004660.g004

the complete F_oF_1-ATPase in the non-induced BF cells. Conspicuously, this activity is absent when ATPaseTb2 RNAi is induced (Fig. 5B).

Loss of ATPaseTb2 disrupts the F_oF_1-ATPase complexes in BF *T. brucei*

The absence of activity for the F_oF_1-monomeric complex might be explained by complex instability. Thus, the structural integrity of the coupled F_oF_1-complex was further analyzed using hrCNE, which were loaded with digitonin-lysed mitochondria from non-induced and ATPaseTb2 RNAi induced cells. After transferring the separated native protein complexes to a nitrocellulose membrane, a specific antibody against the p18 subunit detected the F_1-moiety as well as both monomeric and oligomeric F_oF_1-complexes (Fig. 5C). Interestingly, we repeatedly observed that the abundance of the monomeric and oligomeric complexes is decreased after RNAi induction and by day 3 these complexes are not detected at all. These results were complemented by the sedimentation profile of F_oF_1-ATPase complexes on glycerol gradients. Mitochondria were isolated from non-induced RNAi cells and cells induced for two days (IND2). These were then lysed by 1% Triton X-100 and an equal amount of mt protein from each sample was fractionated on a 10–30% GG. The resolved fractions were then analyzed by western blot and the anti-β and anti-p18 antibodies demonstrated the effect of the ATPaseTb2 KD on the F_oF_1-ATPase sedimentation profile. As indicated in Fig. 5D and the corresponding scanning densitometry results listed in S2 Fig., two days of RNAi induction resulted in a diminished amount of β and p18 signals from the higher S-values (IND2 panels), while the GG sedimentation pattern of RNAi non-induced cells was more similar to wild type BF427 (see Fig. 3C). These results are in agreement with the PF RNAi ATPaseTb2 cell lines, in which the stability of the monomeric and multimeric F_oF_1-ATP synthases was significantly affected upon RNAi [26].

Using a variety of methods employing various detergent types, we have established that the ATPaseTb2 subunit is an essential component of the F_oF_1-ATPase monomer and higher oligomers in the bloodstream stage of *T. brucei*. Furthermore, the depletion of ATPaseTb2 diminishes the abundance of membrane-bound F_oF_1-ATPase complexes, which directly initiates a substantial decrease in the $\Delta\psi_m$ that manifests as a strong growth phenotype.

ATPaseTb2 depletion affects cell growth, the $\Delta\psi_m$ and F_oF_1-ATPase integrity in Dk *T. b. evansi*

To further dissect the primary role of the membrane-bound ATPaseTb2 subunit, we investigated the effect of targeted gene silencing in transgenic Dk *T. b. evansi*, which facilitate the tet

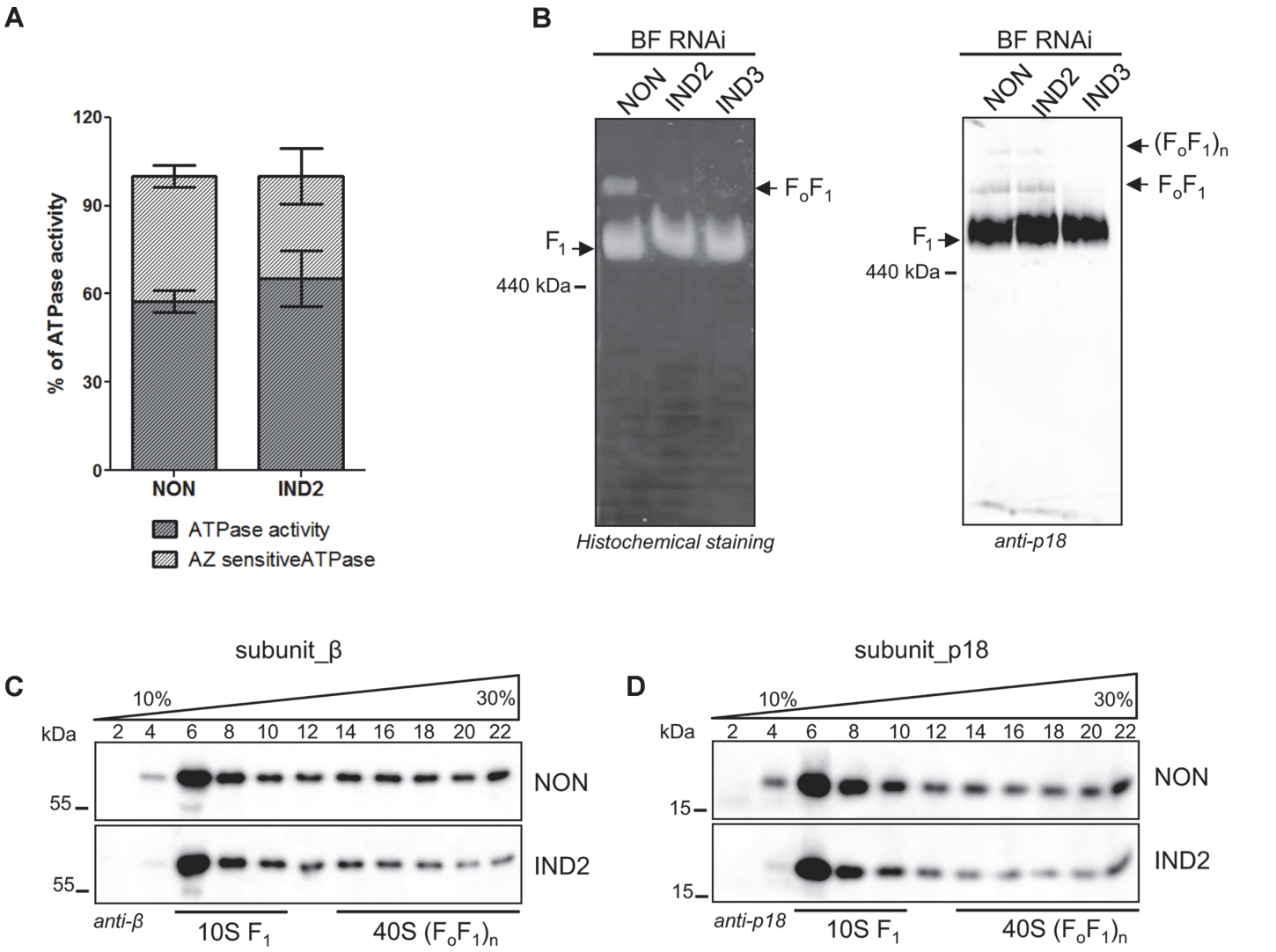

Fig 5. ATPaseTb2 depletion does not appreciably affect F_1-ATPase activity in BF *T. brucei* cells, but it does significantly diminish the stability of F_oF_1-ATPase complexes. A) Employing the Sumner ATPase assay, the F_1-ATPase hydrolytic activity was measured in ATPaseTb2 RNAi cells either not induced (NON) or induced for 2 days (IND2). Crude mt vesicles were obtained by digitonin extraction and the ATPase activity was assayed by measuring the release of free phosphates. The specific F_1-ATPase inhibitor, azide (AZ, 2 mM), was added as indicated. The total amount of free-phosphate created from all ATPase enzymes present in the sample was set at 100% (hatched column). The azide-sensitive activity representing the F_1-ATPase is depicted in dark grey. The results are means ± s.d. (n = 4). B) In-gel ATP hydrolysis activity of F_oF_1-ATPase was visualized after ATPaseTb2 reduction. Mitochondria from RNAi non-induced cells (NON) and cells induced for 2 (IND2) and 3 (IND3) days were lysed with 2% dodecyl maltoside. Equal amounts of lysed mitochondrial proteins (100 μg) were fractionated on a 2%-12% BNE and the F_oF_1-ATPase activity was visualized by in-gel histochemical staining resulting in a white lead phosphate precipitate. Positions of F_1-ATPase and monomeric F_oF_1-ATPase are depicted. The size of equine spleen ferritin (440 kDa) is indicated. C) The stability of F_oF_1-ATPase complexes upon ATPaseTb2 silencing was examined using hrCNE. Mitochondria from RNAi non-induced cells (NON) and cells induced for 2 (IND2) and 3 (IND3) days were lysed by digitonin (4 mg/mg). Equal amounts of lysed mitochondrial proteins (20 μg) were fractionated on a 3%-12% hrCNE, blotted onto a nitrocellulose membrane and probed with the anti-p18 antibody. Positions of F_1-ATPase and monomeric and dimeric F_oF_1-ATPases are depicted by arrows. The size of ferritin from equine spleen (440 kDa) is indicated. D) The sedimentation profile of F_oF_1-ATPase complexes was examined using western blot analysis of glycerol gradient fractions. Mitochondria from RNAi non-induced cells (NON) and cells induced for 2 days (IND2) were lysed with 1% Triton X-100. An equal amount of the cleared lysates (3,3 mg) were loaded on a manually poured 10–30% glycerol gradient. Western analyzes with anti-β and anti-p18 antibodies depicted the sedimentation profile of the F_oF_1-ATPase complexes. The manually fractionated glycerol gradient fractions are labelled and sizes of the protein marker are indicated.

doi:10.1371/journal.ppat.1004660.g005

inducible expression of dsRNA. These Dk cells were transfected with an ATPaseTb2 RNAi vector and several positive clones were screened for a growth phenotype. As shown in Fig. 6A, the surprising inhibition of cell growth in RNAi induced cells appeared two days after tet induction

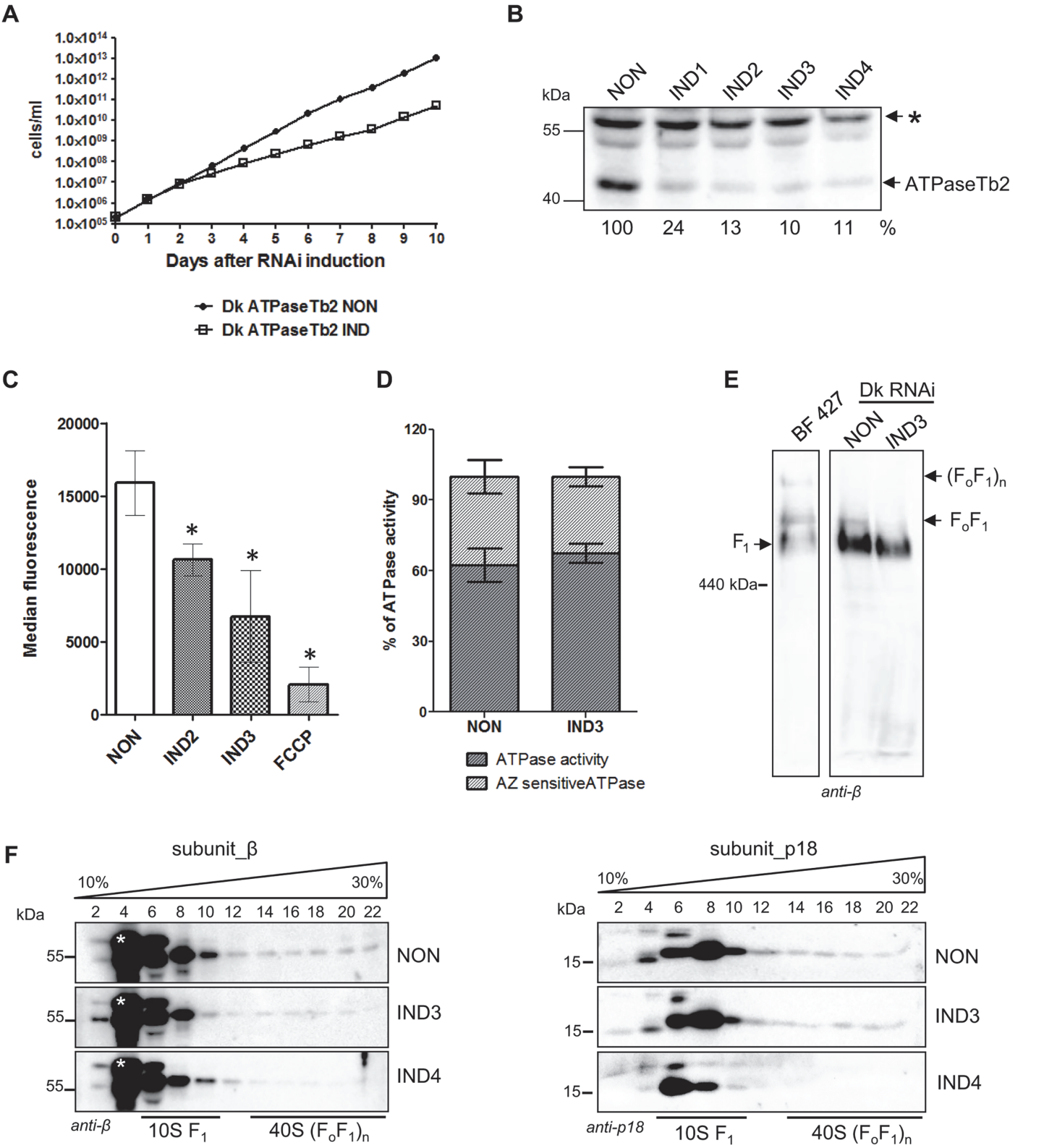

Fig 6. Cell growth, $\Delta\psi_m$ maintenance and the stability of FoF1-ATPase complexes are all affected by the loss of ATPaseTb2 in dyskinetoplastic *T.b. evansi.* A) Growth curves of the non-induced (NON) and induced (IND) ATPaseTb2 RNAi Dk *T. b. evansi* cell lines were measured for 10 days. Cells were maintained in the exponential growth phase (between 10^5 and 10^6 cells/ml) and the cumulative cell number represents the cell density adjusted by the daily dilution factor. The figure is representative of three independent RNAi-inductions. B) The steady-state abundance of ATPaseTb2 in non-induced (NON)

cells and cells harvested 1, 2, 3 and 4 days post RNAi induction (IND1, IND2, IND3, IND4) was determined by western blot analysis using a specific ATPaseTb2 antibody. Mt Hsp70 served as a loading control. The numbers underneath the ATPaseTb2 panel represent the abundance of immunodetected protein expressed as a percentage of the non-induced samples after normalizing to the loading control. The pertinent sizes of the protein marker are indicated on the left. The figure is a representative western blot from three independent RNAi-inductions. C) The $\Delta\psi_m$ was measured in non-induced (NON) ATPaseTb2 RNAi cells and cells induced for 2 and 3 days (IND2 and IND3) by flow cytometry using Mitotracker Red CMX-Ros. The results are means ± s.d. (n = 3). *$P < 0.05$, Student's *t*-test. D) The F_1-ATPase hydrolytic activity was measured for induced (IND3) or non-induced Dk ATPaseTb2 RNAi cells as described in Fig. 5A. The results are means ± s.d. (n = 4). E) The stability of F_oF_1-ATPase complexes upon ATPaseTb2 depletion was examined using hrCNE. Mitochondria from wild type BF427, ATPaseTb2 RNAi *T. b. evansi* non-induced cells (NON) and cells induced for 3 days (IND3) were lysed by digitonin (4 mg/mg). Equal amounts of lysed mitochondrial proteins (20 μg) were fractionated on a 3%-12% hrCNE, blotted onto a nitrocellulose membrane and probed with an anti-β antibody. Positions of F_1-ATPase and monomeric and multimeric F_oF_1-ATPases are depicted by arrows. The size of the equine spleen ferritin (440 kDa) is indicated on the left. F) The sedimentation profile of F_oF_1-ATPase complexes was examined using western blot analysis of glycerol gradient fractions. Mitochondria from RNAi non-induced cells (NON) and cells induced for 3 and 4 days (IND3 and IND4) were lysed by 1% Triton X-100 and an equal amount of the cleared samples (1.3 mg) were loaded on a 10–30% glycerol gradient. Western analyzes with anti-β and anti-p18 antibodies depicted the sedimentation profile of the F_oF_1-ATPase complexes. The glycerol gradient fractions are labelled and the relevant sizes of the protein marker are indicated. A nonspecific band only visible in Dk164 gradients is indicated by an asterisk.

doi:10.1371/journal.ppat.1004660.g006

and the doubling time remained reduced throughout the whole ten day experiment. Furthermore, western analysis of whole cell lysates harvested over the RNAi time course exhibited a significant reduction of ATPaseTb2 in the RNAi induced cells beginning on day 1 (Fig. 6B), while the analysis of a non-specific band served as the loading control. Interestingly, if the only role of the subunit was to stabilize the proton pore, it presumably would not be essential in cells that lack mtDNA and have adapted to the loss of a functioning proton pore. However, these results suggest that ATPaseTb2 is important for F_oF_1-ATPase complexes in these unique cells and thus this cell line was further exploited to characterize the function of ATPaseTb2.

Since the $\Delta\psi_m$ in Dk cells is generated using the hydrolytic activity of the F_1-moiety coupled with ATP/ADP translocation, the $\Delta\psi_m$ was examined in ATPaseTb2 non-induced and RNAi induced cell populations. As shown in Fig. 6C, a reduction of the $\Delta\psi_m$ was detected in the RNAi induced cell population after 2 (IND2) and 3 days (IND3). Since the reduction of the $\Delta\psi_m$ already appears at day 2 of tet induction and the growth phenotype does not truly manifest until day 3, we postulate that the observed decrease of the $\Delta\psi_m$ is a direct effect of ATPaseTb2 silencing and not a consequence of decreased cell viability. Furthermore, to assess if this decreased $\Delta\psi_m$ is caused by an impairment of the F_1-ATPase hydrolytic activity, the total ATPase activity was measured in mt lysates with or without azide. Similar to BF RNAi ATPaseTb2 cells (Fig. 5A), no changes in total or azide-sensitive activities were observed between the non-induced and ATPaseTb2 RNAi-induced cells (Fig. 6D).

The structural integrity of Dk F_oF_1-ATPase complexes was then investigated using mild non-denaturing hrCNE to fractionate mitochondrial proteins purified from BF427 cells and Dk cells either induced for ATPaseTb2 RNAi or not. A western blot containing BF427 mitochondria as a reference sample was probed with an anti-β antibody and used as marker to visualize each state of the F_1-moiety, either isolated by itself or being partnered with the monomeric and multimeric F_oF_1-complexes. Strikingly, while a majority of the β subunit signal in Dk RNAi non-induced cells was observed in the region of isolated F_1-ATPase, we also consistently detected an irrefutable signal corresponding to the F_oF_1-monomeric complex, presumably assembled intact with the exception of subunit a (Fig. 6E). While there is evidence of mammalian rho cells containing a similar complex [44–46], this is the first time it has been demonstrated in the comparable Dk trypanosomatids. Furthermore, the induction of ATPaseTb2 RNAi in the Dk cells led to the disappearance of the monomeric complex, leaving only the F_1-ATPase to be detected on the western blot (Fig. 6E). Once again, the evidence indicates that ATPaseTb2 is important for the structural integrity of the F_oF_1-ATPase and its depletion in Dk *T.b. evansi* cells leads to the disruption of the unique membrane-bound F_oF_1-ATPase complexes.

To corroborate this observation, we purified mitochondria from Dk *T. b. evansi* non-induced and ATPaseTb2 RNAi-induced cells and lysed them with Triton X-100. These gently disrupted lysates were then fractionated on glycerol gradients, which revealed that a majority of the signal from subunits β and p18 was located within fractions 6–10, representing the F_1-moiety (Fig. 6F). Nevertheless, weaker bands representing the F_oF_1-ATPase complexes (fractions 14–22) were again detected in the non-induced samples (Fig. 6F NON panels). Noticeably, these same protein markers in the mt fractionation of ATPaseTb2 RNAi induced cells displayed a significant reduction in fractions 14–22 (Fig. 6F IND4 panels), where the F_oF_1-monomer/oligomer sediments. This observation is quite surprising since the main role of this enzyme is to create the $\Delta\psi_m$, presumably using only the hydrolytic activity of the matrix facing F_1-moiety. In an attempt to determine if a portion of the F_1-ATPase is membrane associated and that the disruption of this attachment is the reason for the observed decrease in the $\Delta\psi_m$ and the detected growth phenotype, we decided to visualize these complexes *in situ* using immunogold labelling followed by electron microscopy.

Loss of ATPaseTb2 leads to the dissociation of F_1-ATPase from the mt membrane

Immunogold labeling with a primary anti-β antibody was performed on ultrasections of Dk *T. b. evansi* non-induced (NON) and ATPaseTb2 RNAi induced cells for 3 (IND3) and 5 (IND5) days. Electron micrographs illustrate that Dk trypanosomes have a simple and reduced mitochondrion (S3A Fig.), lacking both cristae and a typical kinetoplast structure, as previously reported for the dyskinetoplastic *T. b. evansi* [17]. Whenever these reduced double-membrane organelles could be unequivocally identified, we tallied the number of immunogold beads either in the close proximity of the mt membrane or in the matrix (S3A Fig.). Strikingly, 70% of the gold particles identified were found associated with the mt membrane in the NON images (S3B Fig.). From the 113 images captured from either NON, IND3 or IND5 samples, we performed a Chi-squared analysis on the immunogold beads associated with the mt membrane to determine if their distribution is random (S3C Fig.). With two degrees of freedom, the calculated $\chi^2 = 43.5$ ($p < 0.0001$), which signifies that the difference between the observed and expected particles was statistically significant. These values were then plotted to determine the relative labelling index ($RLI = N_{obs}/ N_{exp}$) for the mt membrane associated gold particles (S3D Fig.). This analysis reveals that the observed number of gold particles found in close proximity to the mt membrane for the NON electron micrographs is significantly greater than if the particles were randomly distributed (RLI = 1), while the opposite is true for the IND5 samples. Since we understand the general subjectivity of this method, we performed this experiment in a blinded study and only considered a gold bead to be associated with the mt membrane if it was in the immediate proximity of the membrane. For the very few scored beads that could potentially fall in a membrane-bound grey zone, it should be noted that the physical distance from the subunit β antigen to the gold particle can be up to 15–20 nm, not to mention that subunit β itself is projected from the membrane by subunit γ by as much as 13 nm [47,48]. Furthermore, very few immunogold beads were detected outside of defined mt structures and each mt image only contained 1–8 immunogold beads (average of 2.4 beads/mt image), suggesting that the labelling was very specific for our abundant mt antigen. It is important to note, that utilizing an assay that does not require the use of any detergents, we demonstrated that a majority of the F_1-ATPase is located within close proximity of the mt membrane and this association is disrupted when ATPaseTb2 is depleted.

Discussion

The *T. brucei* F_oF_1-ATPase has obtained unique properties in comparison to its eukaryotic counterparts. The occurrence of novel subunits combined with the lack of typical eukaryotic subunits that compose the F_o membrane-bound moiety and the peripheral stalk is intriguing from an evolutionary viewpoint. Because these atypical subunits lack significant homology to known proteins, questions arise concerning their authenticity as genuine subunits of the complex and what their function and localization within the complex might be. Here, we focused on the functional characterization of one of the trypanosomatid specific subunits, ATPaseTb2 in the bloodstream stages of *T. brucei*. Notably, we determined that its function is essential for maintaining the normal growth rate of the infectious stage of *T. brucei* and also for the important veterinary dyskinetoplastic parasite, *T. b. evansi*. Additional analyses demonstrated that the ATPaseTb2 is membrane embedded and a component of the F_oF_1-ATPase that is present in both BF and Dk cells. Furthermore, the depletion of this F_o-moiety subunit results in a decreased $\Delta\psi_m$ and a loss of F_oF_1-ATPase complexes. Combined with bioinformatic tools that predict a transmembrane domain and identify a low homology to subunit d, we suggest that ATPaseTb2 might be a component of the peripheral stalk of the F_oF_1-ATPase.

The peripheral stalk is indispensable for ATP synthesis as it serves to impede the movement of the catalytic $\alpha_3\beta_3$ headpiece while the proton motive force rotates the c-ring and the connected asymmetrical central stalk in a way that imposes conformational changes in the catalytic nucleotide binding sites of the β subunits. The peripheral stator is also essential when the complex harnesses the energy provided from ATP hydrolysis to drive the rotation of the enzyme in reverse, allowing protons to be pumped across the mt inner membrane to produce the $\Delta\psi_m$ when physiological conditions dictate.

The bovine and yeast peripheral stalk is composed of four subunits, OSCP, b, d, and F_6/h (bovine/yeast nomenclature). Subunit b (~ 20kDa protein) contains two trans-membrane segments at the N-terminus, while the rest of the protein is hydrophilic—protruding into the matrix and interacting with OSCP and subunit d [23,49–51]. The interaction between subunit b and OSCP is stabilized by subunit F_6 [22]. The predominantly hydrophilic subunit d interacts with all three mentioned subunits and it has been shown to be essential for the function of the F_oF_1-complex. The yeast knock-out of subunit d was characterized by the de-attachment of the catalytic F_1-ATPase from the protonophoric sector, the loss of detectable oligomycin sensitive ATPase activity and the absence of subunit a in the F_o-moiety [36]. Notably, of these four subunits, the only homolog identified in the *T. brucei* genome is OSCP and its protein product was identified as a bona fide subunit of the purified F_oF_1-ATP synthase [26]. Homologs for subunits b, d, and F_6 are missing and most likely have been replaced by the novel proteins that associate with the *T. brucei* F_oF_1-ATP synthase. Here we demonstrated that the ATPaseTb2 subunit is a membrane-bound protein, containing one predicted transmembrane domain, with a large hydrophilic region extending into the matrix that possesses a low homology to the bovine subunit d. In accordance with other yeast or bovine subunits of the peripheral stalk, the down-regulation of ATPaseTb2 affects the stability of the F_oF_1-complex and its oligomycin sensitivity (this study, [26]).

Considering the relatively large molecular mass of ATPaseTb2 (43 kDa), it is plausible to speculate that ATPaseTb2 functionally represents the membrane-bound subunit of the peripheral stalk fused with subunit d, offering an early attempt by eukaryotes to add layers of complexity that will allow for greater adaptability. It is noteworthy to mention that a species-specific architectural variant of the peripheral stalk was also proposed for colorless and green algae, where the novel subunits Asa2, Asa4 and Asa7 fulfil a structural role in forming the peripheral stalk [52,53]. Other discrepancies from the typical eukaryotic enzyme model can be

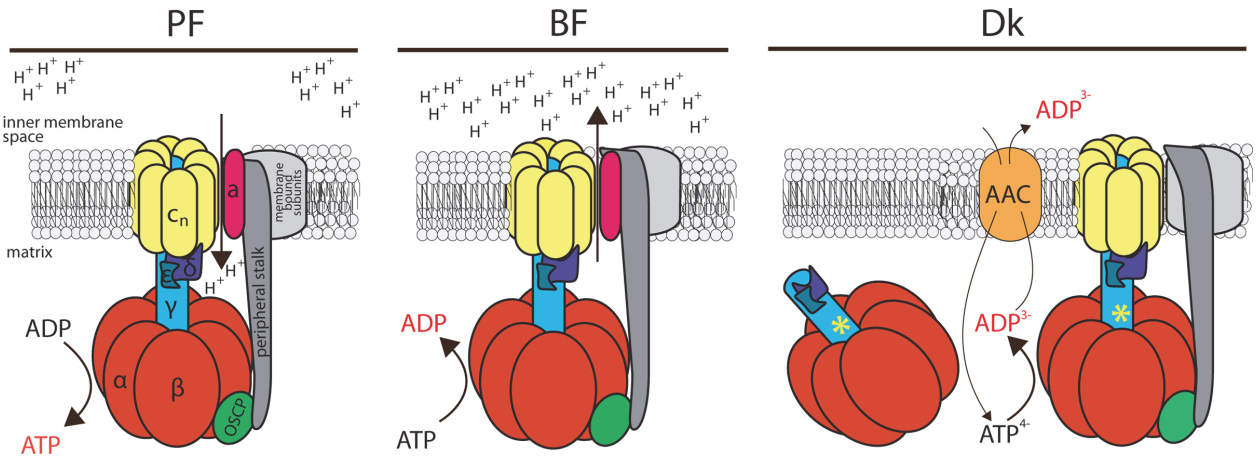

Fig 7. Schematic representation of the F_oF_1-ATP synthase/ATPase complex in trypanosome mitochondria. The F_oF_1-ATP synthase possesses the conventional function in the procyclic form (PF) of the parasite, coupling transmembrane proton transfer with ATP synthesis. In contrast, this enzymatic complex works in reverse in the bloodstream form (BF) of the parasite, hydrolyzing ATP to generate the $\Delta\psi_m$ in the absence of canonical cytochrome-containing respiratory complexes. This hydrolytic activity is also utilized in the dyskinetoplastid (Dk) form, which lacks mitochondrial DNA and thus a proton pore. Therefore, in Dk cells, enhanced ATP hydrolysis by a mutated F_1-moiety (a necessary mutation in the γ subunit is marked with the asterisk) provides substrate for the ATP/ADP carrier (AAC) and the $\Delta\psi_m$ is produced by the electrogenic exchange of ADP^{3-} for ATP^{4-}. Furthermore, we present that a minor fraction of F_1-ATPase still appears to be associated with F_o and that association may be functionally important for maintaining the $\Delta\psi_m$. Orthologues of the colored subunits (α, β, γ, δ, ε, OSCP, a and c) have been annotated in trypanosomes. In addition to OSCP, the peripheral stalk (dark grey) is usually composed of subunits b, F_6 and d, but these homologs have not been identified in the *T. brucei* genome. Also, conspicuously absent are subunits A6L, e, f and g, which are all membrane-bound (light grey).

doi:10.1371/journal.ppat.1004660.g007

found in the ciliate *Tetrahymena thermophila*, representing the superphylum of Alveolates, where the homolog of the conserved subunit b has so far not been identified in the genome. Instead, three novel proteins detected in this ATP synthase complex have been proposed to substitute for subunit b [28]. Thus, it seems that the composition and overall structural appearance of the F_oF_1-ATP synthase from organisms representing different lineages other than Opisthokonts, might be more diverse than previously thought and deserve more attention from basic researchers to elucidate alternate evolutionary solutions to a common thread of life.

T. brucei is a member of the Excavata clade and represents a desirable model to study the function and regulation of the F_oF_1-ATP synthase/ase complex since it utilizes the proton motive force to produce ATP in the PF life stage, while in the BF stage it hydrolyzes ATP to pump the protons necessary to create the $\Delta\psi_m$. Moreover, dyskinetoplastic *T. b. evansi* employs the hydrolytic activity of the F_1-ATPase and the electrogenic exchange of ADP^{3-} for ATP^{4-} by the AAC as yet another strategy to generate the $\Delta\psi_m$ (Fig. 7). Therefore, it was surprising that the ATPaseTb2 protein was detected in all four examined cell types (PF, BF, Dk 164 and *T. b. evansi*), albeit at a much lower abundance in BF and Dk cells, but that is in full agreement with the reduced mitochondria previously defined for these two forms [39]. Furthermore, when PF and BF mt lysates were resolved by GG and hrCNE, ATPaseTb2 was only detected when co-localized with the monomeric and oligomeric F_oF_1-ATP synthase/ase complexes. Interestingly, similar results were obtained from the mt lysates of cells lacking mtDNA. Considering that only the F_1-ATPase was previously assumed to be important for maintaining the $\Delta\psi_m$ in the Dk trypanosomes, the presence of these complexes is intriguing. Nevertheless, a proteomics study performed with osteosarcoma 143B ρ° cells revealed that in addition to the F_1-ATPase subunits, subunit d of the peripheral stalk was also identified [54]. In a similar project involving fibroblast MRC5 ρ° cells, the oligomycin insensitive complex was purified and determined to contain several F_o (b and c) subunits along with a couple of peripheral stalk subunits (OSCP, d). Notably, this complex was loosely associated with the mt membrane [45]. Furthermore,

several additional studies have shown that the F_1-ATPase in yeast or mammalian cells lacking a mt genome (i.e. mammalian subunits a/ATP6, A6L; yeast subunits 6, 8 and 9) is membrane associated, with the attachment most likely occurring via the central and/or peripheral stalk [44,46,55,56]. Our data also suggest that since ATPaseTb2 membrane-bound complexes (monomeric and multimeric) do not display significant differences in their native size or sedimentation values, then the mt encoded subunit a might be the only missing subunit from these complexes. Such a uniquely structured complex can be explained by the current model for the assembly of the F_oF_1-ATPase, in which the F_o subunit a is the last protein incorporated into the enzyme to ensure that it is able to function properly before introducing a complete proton pore. Furthermore, this integration is dependent on the presence of subunit b of the peripheral stalk [57].

RNAi silencing of ATPaseTb2 in BF cells caused a strong growth phenotype concurring with a decreased $\Delta\psi_m$. Importantly, ATPaseTb2 also proved to be essential for maintaining the normal growth rate and the $\Delta\psi_m$ of Dk cells. Combined with the hrCNE and glycerol gradient sedimentation assays that revealed a decrease of the high molecular weight complexes, but not the F_1-ATPase, our studies suggest that these membrane-bound enzymes might significantly contribute to the membrane potential in Dk cells. The biological significance of this localization of the F_1-ATPase might be to efficiently coordinate the activity of this enzyme with its substrate transporter, both of which are responsible for producing the $\Delta\psi_m$ in Dk. By restricting the F_1-ATPase to the mt membrane, it keeps it within the close vicinity of its biochemically functional partner, the AAC. In this way, it helps ensure that the hydrolysis of ATP results in a relatively concentrated region of substrate for the mt membrane embedded AAC, especially in a mitochondrion lacking defined cristae and the microenvironments they create. Indeed, there is precedence for such a close spatial collaboration to increase efficiency, as an actual physical interaction between these two enzymes has been reported as the ATP synthasome in mammals [40,58]. We are currently building a set of tools to perform additional functional assays and imaging techniques that we hope will further resolve the function of the F_oF_1-ATPase complexes in these pathogenic trypanosomes.

Materials and Methods

Plasmid construction

The ATPaseTb2 (Tb927.5.2930) RNAi constructs targeted an 825 bp fragment of the gene that was PCR amplified from *T. brucei* strain 427 genomic DNA with the following oligonucleotides: FW—CACGGATCCATGCGCCGTGTATC, REV-CACCTCGAGTTCGGCCCGATC. Utilizing the BamHI and XhoI restriction sites inherent in the primers (underlined), this fragment was cloned into the p2T7-TA blue plasmid [59] (used to create a BF RNAi cell line) and the p2T7–177 plasmid [60] (used to generate a Dk RNAi cell line). For the inducible expression of ATPaseTb2 fused with a C-terminal 3xv5 tag, the ATPaseTb2 coding sequence was PCR amplified (Fw: ACAAAGCTTATGC GCCGTGTATC, Rev: ATAGGATCCGTG ATGGGCCTTTTTC) and cloned into the pT7_v5 vector using HindIII and BamHI restriction enzymes [61]. The pLEW79MHTAP vectors for the tet inducible expression of ATPaseTb2 and Tb927.5.1710 (F_oF_1-ATPase subunit p18) TAP-tagged proteins were previously described in [26].

Trypanosoma culture conditions and generation of cell lines

Bloodstream form *T. brucei brucei* Lister 427 strain, stable acriflavin-induced dyskinetoplastic *T. b. brucei* EATRO 164 [18] and dyskinetoplastic *T. b. evansi* Antat 3/3 [62] were all grown *in vitro* at 37°C and 5% CO_2 in HMI-9 media containing 10% FBS. The BF427 single marker cell

line [63] and a *T. b. evansi* cell line [14], both constitutively expressing the ectopic T7 RNA polymerase and tet repressor (TetR were used for the tet inducible expression of dsRNA and the TAP- and v5-tagged proteins. Each plasmid was linearized with NotI enzyme and transfected into the appropriate cell line as described previously [63]. Linearized p2T7–177 was targeted to the minichromosome 177 basepair repeat region, while linear pTv5 and pLEW79MHTAP vectors were integrated into the rDNA intergenic spacer region [60,61,63]. The induction of RNAi and ectopically expressed tagged proteins was triggered by the addition of 1 μg/ml of tet into the media. Cell densities were measured using the Z2 Cell Counter (Beckman Coulter Inc.). Throughout the analyses, cells were maintained in the exponential mid-log growth phase (between $1x10^5$ to $1x10^6$ cells/ml).

Tandem affinity purification (TAP) of tagged complexes

The TAP protocol was generously provided by L. Jeacock and A. Schnaufer (personal communication) and optimized for BF cells. Briefly, $2x10^8$ cells were harvested and lysed for 20 min on ice with 1% Triton X-100 in an IPP150 buffer (150 mM NaCl, 0,1% NP40, 10mM Tris-HCl pH 8.0) containing Complete protease inhibitors (Roche). The lysates were then cleared by centrifugation (16,000 g, 15 min, 4°C). Meanwhile, IgG antibodies were covalently bound to Dynabeads M-270 Epoxy (Invitrogen) using a protocol previously described [64]. Charged beads were blocked with 1% BSA and then incubated with the cleared cell lysates (4°C for 2 hours, constantly rotating). The beads were then washed three times with IPP150 and once with a TEVCB buffer (150 mM NaCl, 0.1% NP40, 0.5 mM EDTA, 1 mM DTT, 10 mM Tris-HCl, pH 8.0). Finally, the bound protein complexes were released by AcTEV protease (Invitrogen) cleavage and the eluate was analyzed by SDS-PAGE.

Isolation of mt vesicles

Crude mt vesicles were obtained by hypotonic lysis as described in detail earlier [65]. Briefly, cell pellets from $\sim 2x10^9$ cells were washed with SBG (150 mM NaCl, 20 mM glucose, 20 mM $NaHPO_4$, pH 7.9), resuspended in DTE (1 mM Tris, 1 mM EDTA, pH 8.0) and homogenized in a Dounce homogenizer. Alternatively, for a smaller scale hypotonic isolation, cell pellets from $\sim 1x10^9$ cells were washed in NET buffer (150 mM NaCl, 100 mM EDTA, 10 mM Tris, pH 8.0), resuspended in DTE and homogenized by passing through a 25G needle. To re-create the physiological isotonic environment, 60% sucrose was immediately added to the lysed cells to reach a final concentration of 250 mM. Samples were spun down at 15,000 g, 10 min, 4°C to clear the soluble cytoplasmic material from the lysates. The resulting pellets were resuspended in STM (250 mM sucrose, 20 mM Tris pH 8.0, 2 mM $MgCl_2$), supplemented with a final concentration of 3 mM $MgCl_2$ and 0.3 mM $CaCl_2$ before incubating with 5 μg/ml DNase I for 1hr on ice. Then an equal volume of STE buffer (250 mM sucrose, 20 mM Tris pH 8.0, 2 mM EDTA pH 8.0) was added and the material was centrifuged at 15,000 g, 10 min, 4°C. Pellets enriched with the mt membrane vesicles were washed in STE and kept at -70°C.

SDS-PAGE and Western blot

Protein samples were separated on SDS-PAGE, blotted onto a PVDF membrane (PALL) and probed with the appropriate monoclonal (mAb) or polyclonal (pAb) antibody. This was followed by incubation with a secondary HRP-conjugated anti-rabbit or anti-mouse antibody (1:2000, BioRad). Proteins were visualized using the Pierce ECL system (Genetica/Biorad) on a ChemiDoc instrument (BioRad). When needed, membranes were stripped at 50°C for 30 min in a stripping buffer (62.5 mM Tris pH 6.8, 100 mM mercapthoethanol, 2% SDS) and reprobed. The PageRuler prestained protein standard (Fermentas) was used to determine the size

of detected bands. Primary antibodies used in this study were: mAb anti-v5 epitope tag (1:2000, Invitrogen), mAb anti-mtHsp70 (1:2000) [66], pAb anti-AAC (1:2000) [67], pAb anti-MRP1 (1:1000) [68], pAb anti-APRT (1:1000) and pAb anti-enolase (1:1000) [69]. Antibodies against ATPaseTb2 (1:1000), ATPaseTb1 (1:1000), subunit β (1:2000) and subunit p18 (1:1000) were prepared for the purpose of this study. The open reading frames of the respective genes without their predicted mt localization signal were cloned into the *E. coli* expression plasmid, pSKB3. The proteins were overexpressed in BL21 *E. coli* cells and purified under native conditions (subunit β) or denatured conditions (ATPaseTb2, ATPaseTb1 and p18) using a 6 M guanidinium lysis buffer and 8 M urea binding buffer. The denatured proteins were then refolded with a step-wise dialysis procedure that included 0.5 M arginine in the refolding buffer. Native and refolded antigens were sent to Pineda (Antikörper-Service, Germany) or Davids Biotechnologie (Regensburg, Germany) for polyclonal antibody production.

Mt membrane potential ($\Delta\psi_m$) measurement

The $\Delta\psi_m$ was determined utilizing the red-fluorescent stain Mitotracker Red CMX-Ros (Invitrogen). Cells in the exponential growth phase were stained with 100 nM of the dye for 30 min at 37°C. Cells were pelleted (1,300 g, 10 min, RT), resuspended in 2 ml of PBS (pH 7.4) and immediately analyzed by flow cytometry (BD FACS Canto II Instrument). For each sample, 10,000 events were collected. Treatment with the protonophore FCCP (20 μM) was used as a control for mt membrane depolarization. Data were evaluated using BD FACSDiva (BD Company) software.

F_1- ATPase assay

ATPase activity was measured with the Sumner assay, which is based on the release of free phosphate when ATP is hydrolyzed by the enzyme as described earlier [14,70]. Briefly, crude mt lysates were obtained from $2x10^8$cells by SoTe/digitonin extraction (0.015% digitonin, 0.6 M Sorbitol, 2 mM EDTA, 20 mM Tris-HCl pH 7.5). Mt pellets were resuspended in an assay buffer (200 mM KCl, 2 mM $MgCl_2$, Tris-HCl pH 8.0) and the 20 min reaction was initiated by the addition of ATP to a final concentration of 5 mM. Where indicated, samples were pre-treated with the F_1-ATPase specific inhibitor, sodium azide (2 mM) for 10 min at 37°C. The 100 μl enzymatic reactions were deproteinated by the addition of 1.9 μl of 70% perchloric acid. After a 30 min incubation on ice, the samples were spun down (16,000g, 10 min, 4°C) and 90 μl of the supernatant was incubated for 10 min with 0,5 ml of Sumner reagent (8.8% $FeSO_4.7H_2O$, 375 mM H_2SO_4, 6.6% $(NH_4)Mo_7O_{24}.4H_2O$)[62]. 200 μl was then transferred to a 96 well plate and the absorbance was measured at 610 nm using a Tecan Infinite plate reader (Infinite M200Pro, Tecan). To calibrate the assay, a standard curve was calculated from the absorbance values of linear inorganic phosphate samples (0–2 mM).

In-gel histochemical staining of F_1-ATPase activity

Blue native PAGE (BNE) of mt lysates, followed by in-gel activity staining was adapted from published protocols [26,32]. Briefly, mt vesicles from $\sim 2x10^9$ cells were resuspended in a mt lysis buffer (0,75 M amino-n-caproic acid—ACA, 50 mM Bis-Tris, 0,5 mM EDTA, pH 7.0), lysed with 2% dodecylmaltoside (DDM) for 1hr on ice and then cleared by centrifugation (16,000g for 30 min, 4°C). The protein concentration of each mt lysate was determined by a Bradford assay (BioRad), so that 100 μg of total mt protein could be mixed with 1 M ACA and 5% Coomassie brilliant blue G-250 before being loaded on a 2–12% Bis-Tris BNE gel. Immediately after the run (3 hr, 100 V, 4°C), the gel was incubated overnight in an ATPase reaction buffer (35 mM Tris pH 8.0, 270 mM glycine, 19mM MgSO4, 0.3% $Pb(NO_3)_2$, 11 mM ATP).

High resolution clear native PAGE (hrCNE)

The protocol for hrCNE was adapted from published studies [71,72]. In summary, crude mt vesicles from $\sim 5x10^8$ cells were resuspended in a mt lysis buffer (2 mM ACA, 50 mM Imidazole-HCl, 1 mM EDTA, 50 mM NaCl, pH 7) and lysed for one hour on ice with 4 mg digitonin/1 mg protein. The samples were spun down at 16,000 g for 30 min and the cleared lysate protein concentrations were determined by a Bradford assay. Samples were mixed with a 5x loading dye (0.1% Ponceau-S, 50% glycerol) and loaded onto a 3%-12% native gradient gel. After electrophoresis (3 hr, 100 V, 4°C), the resolved mt lysates were transferred onto a nitrocellulose membrane (overnight, 20 V, 4°C) and probed with selected antibodies.

Na_2CO_3 submitochondrial fractionation

Na_2CO_3 extraction of mt membranes was adapted from a previously published protocol [73]. Mt vesicles from $1x10^9$ cells were isolated by hypotonic lysis as described above. The resulting supernatant from the 25G needle homogenization step was kept as a cytosolic fraction (CYTO). The mt pellet was further treated with digitonin (80 μg/ml) for 15 min on ice to disrupt the mt outer membrane. The material was then cleared by centrifugation (12,000 g, 20 min, 4°C) and the pelleted mitoplasts were resuspended in 0.1 M Na_2CO_3 buffer (pH 11.5) and incubated for 30 min on ice. A final ultracentrifugation step (100,000 g, 4°C for 1 hr) performed in an SW50Ti rotor of a Beckman Instrument resulted in a supernatant comprised of proteins from the mt matrix (MX), including stripped peripheral membrane proteins, and a pellet containing integral proteins isolated from the mt membrane fraction (M).

Glycerol gradient (GG) sedimentation

Hypotonically purified mt vesicles from $\sim 2.5x10^9$ cells were resuspended in a GG lysis buffer (10 mM Tris, pH 7.2, 10 mM $MgCl_2$, 200 mM KCl, 1mM DTT) and lysed with 1% Triton X-100 (30 min, on ice). The lysates were cleared by a centrifugation step (2x 16,000 g, 30 min, 4°C) and the protein concentration was determined by a Bradford assay. Mt cleared lysates were resolved by ultracentrifugation (Beckman Instrument, SW40 rotor) at 38,000 g for 5 hr on 11ml 10–30% GG, which was poured manually or using the Gradient Station (Biocomp) according to the manufacturer's protocol. The glycerol gradients were then fractionated either manually or with the Gradient station and 500μl fractions were stored at -70°C.

Immunogold staining of ultrathin sections and transmission electron microscopy

Cells ($\sim 5x10^7$) were pelleted (1300 g, 10 min, RT), washed in PBS (pH 7.4) and immediately fixed in a 4% formaldehyde/ 0.1 M phosphate buffer. Samples were then dehydrated at -10°C through a series of seven steps that increased the concentration of ethanol from 30% to100%, pausing at each step for 1 hour. Next, the samples were embedded in LR White Resin (Electron Microscopy Sciences) and polymerized (UV light, 48 hours at -10°C). Ultrathin sections were prepared by the Ultracut UCT ultramicrotome (Leica) and mounted on nickel grids. Prepared sections were blocked in 5% BSA, labelled with primary anti-β antibody (1:10 dilution), washed three times with PBS and incubated with protein A conjugated to 10 nm gold particles (1:100 dilution, Aurion). The immunogold labelled grids were contrasted, carbon coated and examined by the TEM (JEM-1010, Jeol). Grids, which were immunolabeled with only the protein A conjugated to 10nM gold particles, were used as a negative control.

Quantification and statistical analysis of immunogold labelling

The number of gold particles was statistically evaluated as described earlier [12,74]. Using ImageJ software (NIH, USA), a grid consisting of squares (test points, P) with constant size (16,105 μm^2) was superimposed randomly on the electron micrographs of identified mitochondria. All test squares and immunogold particles within the immediate proximity to the mt membrane were counted separately for each micrograph. In order to statistically evaluate the labelling, all observed gold particles (N_{obs}) and all test points (P) from 113 images captured from NON, IND3 and IND5 samples were tallied. Expected numbers of gold particles (N_{exp}) for each sample were calculated as (total sum N_{obs} x P)/total sum P. To determine if the difference between the observed and expected particles was significant and not due to random fluctuations, a Chi-squared analysis $\chi^2 = (N_{obs}—N_{exp})^2/ N_{exp}$ was performed using GraphPad QuickCalcs calculator (www.graphpad.com/quickcalcs). In addition, the relative labeling index (RLI), where the predicted RLI = 1 for random labelling, was calculated as RLI = N_{obs}/ N_{exp}.

Gene IDs for the genes and proteins mentioned in this study

ATPaseTb2 (Tb927.5.2930), ATPaseTb1 (Tb927.10.520), TbAAC (Tb927.10.14820/30/40), p18 (Tb927.5.1710), mtHsp70 (Tb927.6.3740), MRP1 (Tb927.11.1710), APRT (Tb927.7.1780), enolase (Tb427.10.2890), subunit β (Tb927.3.1380).

Supporting Information

S1 Fig. Bioinformatics analysis of ATPaseTb2. A) The multiple sequence alignment of ATPaseTb2 homologs from the order Kinetoplastida was performed by ClustalW on the following species (accession number, name): *Trypanosoma vivax* Y486 (TvY486_0502300, ATPaseTv2), *T. cruzi* Sylvio X10/1 (TCSYLVIO_010784, ATPaseTc2), *T. congolense* IL3000 (TcIL3000_5_3200, ATPaseTco2), *T. cruzi* CL Brener Non-Esmeraldo-like (TcCLB.506321.280, ATPaseTcB2), *T. cruzi* marinkellei strain B7 (Tc_MARK_9008, ATPaseTcm2), *T. brucei* TREU927 (Tb927.5.2930, ATPaseTb2), *L. tarentolae* Parrot-TarII (LtaP08.0840, ATPaseLt2), *L. mexicana* MHOM/GT/2001/U1103 (LmxM.08.1100, ATPaseLmx2), *L.major* strain Friedlin (LmjF.08.1100, ATPaseLm2), *L. infantum* JPCM5 (LinJ.08.1010, ATPaseLin2), *L. donovani* BPK282A1 (LdBPK_081010.1, ATPaseLd2), *L. braziliensis* MHOM/BR/75/M2904 (LbrM.08.0870, ATPaseLbr2), *Bodo saltans* (ATPaseBs2), *Strigomonas culicis* (STCU_02070, ATPaseSc2). Sequences were obtained from GeneDB database or from Welcome Trust Sanger centrum (*B. saltans* sequence). Numbers at the top indicate the amino acid positions in *T. vivax* ATPaseTv2. The mitochondrial targeting signal for ATPaseTb2 (MTS, green) was predicted by Mitoprot II v1.101. The homologous region (red) to Bs_sub d was determined using HHpred toolkit. B) The homology of ATPaseTb2 to subunit d (*B. taurus*) was based on HHpred, which utilizes the homology detection & structure prediction by HMM-HMM comparison. (http://toolkit.tuebingen.mpg.de) The alignments consist of one or more blocks with the following lines: ss_pred: query secondary structure as predicted by PSIPRED (upper case letters: high probability, lower case letters: low probability). Q query_name: query sequence Q Consensus: query alignment consensus sequence Quality of colum-column match: very bad =; bad—; neutral.; good +; very good |T Consensus: template alignment consensus sequence T templ_name: template sequence T ss_dssp: template secondary structure as determined by DSSP T ss_pred: template secondary structure as predicted by PSIPRED (upper case letters: high probability, lower case letters: low probability) The consensus sequence uses capital letters for amino acids that occur with > = 60% probability and lower case letters for amino acids that have > = 40% probability. For unconserved columns a tilde is used. The line in the middle shows the column score between the query and template amino

acid distributions. It gives a valuable indication for the alignment quality. (A unit of column score corresponds approximately to 0.6 bits.)
=: very bad match column score below-1.5
-: bad match column score between-1.5 and-0.5
.: neutral match column score between -0.5 and +0.5
+: good match column score between +0.5 and +1.5
|: very good match column score above +1.5
(PDF)

S2 Fig. Densitometric analysis of anti-sub_β and anti-p18 immunoblots of the BF ATPaseTb2 RNAi glycerol gradients depicted in Fig. 5D. The glycerol gradient fractions analyzed by western blot using anti-β (A) and anti-p18 (B) antibodies (Fig. 5D) were also examined using densitometry analysis. The chemiluminescent blots were imaged with the LAS3000 Imaging System (FUJI). The specific bands for subunit β and p18 were selected using the band analysis tool from the ImageQuant TL software (Amersham Biosciences), which allowed their background-subtracted densities to be determined. The background-corrected volumes of the corresponding protein bands were normalized to the highest value of each blot, which was set to 100.
(PDF)

S3 Fig. ATPaseTb2 depletion alters the distribution of the F_1-ATPase subunit β in *T.b. evansi* mitochondria. A) Ultrathin sections of RNAi non-induced cells (NON) and cells induced for 3 (IND3) and 5 (IND5) days were immunostained with a primary anti-β antibody, followed by incubation with a 10 nM gold bead conjugated anti-protein A secondary antibody. Images of the electron micrographs were captured and the immunogold particles visualized within identified mitochondria. Particles located in the matrix are marked with dashed arrows, while gold beads located within the immediate proximity of the mt membrane are designated with a solid arrow. B) All immunogold beads identified from 113 images of NON, IND3 and IND5 electron micrographs were itemized according to their localization and plotted as either mt inner membrane associated (grey) or matrix (white). C) Counts of observed mt membrane associated gold particles (N_{obs}) and all test points (P) from NON, IND3 and IND5 images were recorded under their appropriate column. Expected numbers of gold particles (N_{exp}) were calculated as (total sum N_{obs} x P)/total sum P. D) The relative labeling index was calculated (RLI = N_{obs}/ N_{exp}) for the mt membrane associated gold particles tabulated in S3B Fig. and is depicted on the y-axis of the column graph.
(PDF)

Acknowledgments

We thank Ken Stuart (Seattle Biomed) and Minu Chaudhuri (Meharri Medical College) for kindly providing antibodies, Achim Schnaufer (University of Edinburgh) for providing the *T. b. evansi* strain used in this study. We would also like to express our gratitude to Marie Vancová from the Laboratory of Electron Microscopy (Biology Centre) for the sample preparation and an opportunity to use the JEM-1010 electron microscope.

Author Contributions

Conceived and designed the experiments: KS BP AZ. Performed the experiments: KS. Analyzed the data: KS BP AZ. Contributed reagents/materials/analysis tools: AZ KS BP. Wrote the paper: AZ BP KS.

References

1. Jamonneau V, Ilboudo H, Kabore J, Kaba D, Koffi M, et al. (2012) Untreated human infections by Trypanosoma brucei gambiense are not 100% fatal. PLoS Negl Trop Dis 6: e1691. doi: 10.1371/journal.pntd.0001691 PMID: 22720107
2. Stuart K, Brun R, Croft S, Fairlamb A, Gurtler RE, et al. (2008) Kinetoplastids: related protozoan pathogens, different diseases. J Clin Invest 118: 1301–1310. doi: 10.1172/JCI33945 PMID: 18382742
3. Steverding D (2008) The history of African trypanosomiasis. Parasit Vectors 1: 3. doi: 10.1186/1756-3305-1-3 PMID: 18275594
4. Bringaud F, Riviere L, Coustou V (2006) Energy metabolism of trypanosomatids: adaptation to available carbon sources. Mol Biochem Parasitol 149: 1–9. PMID: 16682088
5. Besteiro S, Barrett MP, Riviere L, Bringaud F (2005) Energy generation in insect stages of Trypanosoma brucei: metabolism in flux. Trends Parasitol 21: 185–191. PMID: 15780841
6. Hannaert V, Bringaud F, Opperdoes FR, Michels PA (2003) Evolution of energy metabolism and its compartmentation in Kinetoplastida. Kinetoplastid Biol Dis 2: 11. PMID: 14613499
7. Brown SV, Hosking P, Li J, Williams N (2006) ATP synthase is responsible for maintaining mitochondrial membrane potential in bloodstream form Trypanosoma brucei. Eukaryot Cell 5: 45–53. PMID: 16400167
8. Guler JL, Kriegova E, Smith TK, Lukes J, Englund PT (2008) Mitochondrial fatty acid synthesis is required for normal mitochondrial morphology and function in Trypanosoma brucei. Mol Microbiol 67: 1125–1142. doi: 10.1111/j.1365-2958.2008.06112.x PMID: 18221265
9. Nolan DP, Voorheis HP (1992) The mitochondrion in bloodstream forms of Trypanosoma brucei is energized by the electrogenic pumping of protons catalysed by the F1F0-ATPase. Eur J Biochem 209: 207–216. PMID: 1327770
10. Huang G, Vercesi AE, Docampo R (2013) Essential regulation of cell bioenergetics in Trypanosoma brucei by the mitochondrial calcium uniporter. Nat Commun 4: 2865. doi: 10.1038/ncomms3865 PMID: 24305511
11. Vercesi AE, Docampo R, Moreno SN (1992) Energization-dependent Ca2+ accumulation in Trypanosoma brucei bloodstream and procyclic trypomastigotes mitochondria. Mol Biochem Parasitol 56: 251–257. PMID: 1484549
12. Kovarova J, Horakova E, Changmai P, Vancova M, Lukes J (2014) Mitochondrial and nucleolar localization of cysteine desulfurase Nfs and the scaffold protein Isu in Trypanosoma brucei. Eukaryot Cell 13: 353–362. doi: 10.1128/EC.00235-13 PMID: 24243795
13. Mazet M, Morand P, Biran M, Bouyssou G, Courtois P, et al. (2013) Revisiting the central metabolism of the bloodstream forms of Trypanosoma brucei: production of acetate in the mitochondrion is essential for parasite viability. PLoS Negl Trop Dis 7: e2587. doi: 10.1371/journal.pntd.0002587 PMID: 24367711
14. Schnaufer A, Clark-Walker GD, Steinberg AG, Stuart K (2005) The F1-ATP synthase complex in bloodstream stage trypanosomes has an unusual and essential function. EMBO J 24: 4029–4040. PMID: 16270030
15. Buchet K, Godinot C (1998) Functional F1-ATPase essential in maintaining growth and membrane potential of human mitochondrial DNA-depleted rho degrees cells. J Biol Chem 273: 22983–22989. PMID: 9722521
16. Dean S, Gould MK, Dewar CE, Schnaufer AC (2013) Single point mutations in ATP synthase compensate for mitochondrial genome loss in trypanosomes. Proc Natl Acad Sci U S A 110: 14741–14746. doi: 10.1073/pnas.1305404110 PMID: 23959897
17. Brun R, Hecker H, Lun ZR (1998) Trypanosoma evansi and T. equiperdum: distribution, biology, treatment and phylogenetic relationship (a review). Vet Parasitol 79: 95–107. PMID: 9806490
18. Stuart KD (1971) Evidence for the retention of kinetoplast DNA in an acriflavine-induced dyskinetoplastic strain of Trypanosoma brucei which replicates the altered central element of the kinetoplast. J Cell Biol 49: 189–195. PMID: 4102002
19. Lai DH, Hashimi H, Lun ZR, Ayala FJ, Lukes J (2008) Adaptations of Trypanosoma brucei to gradual loss of kinetoplast DNA: Trypanosoma equiperdum and Trypanosoma evansi are petite mutants of T. brucei. Proc Natl Acad Sci U S A 105: 1999–2004. doi: 10.1073/pnas.0711799105 PMID: 18245376
20. Walker JE (2013) The ATP synthase: the understood, the uncertain and the unknown. Biochem Soc Trans 41: 1–16. doi: 10.1042/BST20110773 PMID: 23356252
21. Devenish RJ, Prescott M, Rodgers AJ (2008) The structure and function of mitochondrial F1F0-ATP synthases. Int Rev Cell Mol Biol 267: 1–58. doi: 10.1016/S1937-6448(08)00601-1 PMID: 18544496

22. Walker JE, Dickson VK (2006) The peripheral stalk of the mitochondrial ATP synthase. Biochim Biophys Acta 1757: 286–296. PMID: 16697972

23. Dickson VK, Silvester JA, Fearnley IM, Leslie AG, Walker JE (2006) On the structure of the stator of the mitochondrial ATP synthase. EMBO J 25: 2911–2918. PMID: 16791136

24. Vaidya AB, Mather MW (2009) Mitochondrial evolution and functions in malaria parasites. Annu Rev Microbiol 63: 249–267. doi: 10.1146/annurev.micro.091208.073424 PMID: 19575561

25. Lapaille M, Escobar-Ramirez A, Degand H, Baurain D, Rodriguez-Salinas E, et al. (2010) Atypical subunit composition of the chlorophycean mitochondrial F1FO-ATP synthase and role of Asa7 protein in stability and oligomycin resistance of the enzyme. Mol Biol Evol 27: 1630–1644. doi: 10.1093/molbev/msq049 PMID: 20156838

26. Zikova A, Schnaufer A, Dalley RA, Panigrahi AK, Stuart KD (2009) The F(0)F(1)-ATP synthase complex contains novel subunits and is essential for procyclic Trypanosoma brucei. PLoS Pathog 5: e1000436. doi: 10.1371/journal.ppat.1000436 PMID: 19436713

27. Mather MW, Henry KW, Vaidya AB (2007) Mitochondrial drug targets in apicomplexan parasites. Curr Drug Targets 8: 49–60. PMID: 17266530

28. Balabaskaran Nina P, Dudkina NV, Kane LA, van Eyk JE, Boekema EJ, et al. (2010) Highly divergent mitochondrial ATP synthase complexes in Tetrahymena thermophila. PLoS Biol 8: e1000418. doi: 10.1371/journal.pbio.1000418 PMID: 20644710

29. Nishi A, Scherbaum OH (1962) Oxidative phosphorylation in synchronized cultures of Tetrahymena pyriformis. Biochim Biophys Acta 65: 419–424. PMID: 13938753

30. Uyemura SA, Luo S, Vieira M, Moreno SN, Docampo R (2004) Oxidative phosphorylation and rotenone-insensitive malate- and NADH-quinone oxidoreductases in Plasmodium yoelii yoelii mitochondria in situ. J Biol Chem 279: 385–393. PMID: 14561763

31. Vazquez-Acevedo M, Cardol P, Cano-Estrada A, Lapaille M, Remacle C, et al. (2006) The mitochondrial ATP synthase of chlorophycean algae contains eight subunits of unknown origin involved in the formation of an atypical stator-stalk and in the dimerization of the complex. J Bioenerg Biomembr 38: 271–282. PMID: 17160464

32. Hashimi H, Benkovicova V, Cermakova P, Lai DH, Horvath A, et al. (2010) The assembly of F(1)F(O)-ATP synthase is disrupted upon interference of RNA editing in Trypanosoma brucei. Int J Parasitol 40: 45–54. doi: 10.1016/j.ijpara.2009.07.005 PMID: 19654010

33. Chi TB, Brown BS, Williams N (1998) Subunit 9 of the mitochondrial ATP synthase of Trypanosoma brucei is nuclearly encoded and developmentally regulated. Mol Biochem Parasitol 92: 29–38. PMID: 9574907

34. Claros MG, Vincens P (1996) Computational method to predict mitochondrially imported proteins and their targeting sequences. Eur J Biochem 241: 779–786. PMID: 8944766

35. Biegert A, Mayer C, Remmert M, Soding J, Lupas AN (2006) The MPI Bioinformatics Toolkit for protein sequence analysis. Nucleic Acids Res 34: W335–339. PMID: 16845021

36. Norais N, Prome D, Velours J (1991) ATP synthase of yeast mitochondria. Characterization of subunit d and sequence analysis of the structural gene ATP7. J Biol Chem 266: 16541–16549. PMID: 1832157

37. Walker JE, Runswick MJ, Poulter L (1987) ATP synthase from bovine mitochondria. The characterization and sequence analysis of two membrane-associated sub-units and of the corresponding cDNAs. J Mol Biol 197: 89–100. PMID: 2890767

38. Nugent T, Jones DT (2009) Transmembrane protein topology prediction using support vector machines. BMC Bioinformatics 10: 159. doi: 10.1186/1471-2105-10-159 PMID: 19470175

39. Vertommen D, Van Roy J, Szikora JP, Rider MH, Michels PA, et al. (2008) Differential expression of glycosomal and mitochondrial proteins in the two major life-cycle stages of Trypanosoma brucei. Mol Biochem Parasitol 158: 189–201. doi: 10.1016/j.molbiopara.2007.12.008 PMID: 18242729

40. Ko YH, Delannoy M, Hullihen J, Chiu W, Pedersen PL (2003) Mitochondrial ATP synthasome. Cristae-enriched membranes and a multiwell detergent screening assay yield dispersed single complexes containing the ATP synthase and carriers for Pi and ADP/ATP. J Biol Chem 278: 12305–12309. PMID: 12560333

41. Meyer B, Wittig I, Trifilieff E, Karas M, Schagger H (2007) Identification of two proteins associated with mammalian ATP synthase. Mol Cell Proteomics 6: 1690–1699. PMID: 17575325

42. Chen Y, Hung CH, Burderer T, Lee GS (2003) Development of RNA interference revertants in Trypanosoma brucei cell lines generated with a double stranded RNA expression construct driven by two opposing promoters. Mol Biochem Parasitol 126: 275–279. PMID: 12615326

43. Bowler MW, Montgomery MG, Leslie AG, Walker JE (2006) How azide inhibits ATP hydrolysis by the F-ATPases. Proc Natl Acad Sci U S A 103: 8646–8649. PMID: 16728506

44. Appleby RD, Porteous WK, Hughes G, James AM, Shannon D, et al. (1999) Quantitation and origin of the mitochondrial membrane potential in human cells lacking mitochondrial DNA. Eur J Biochem 262: 108–116. PMID: 10231371

45. Garcia JJ, Ogilvie I, Robinson BH, Capaldi RA (2000) Structure, functioning, and assembly of the ATP synthase in cells from patients with the T8993G mitochondrial DNA mutation—Comparison with the enzyme in Rho(0) cells completely lacking mtDNA. Journal of Biological Chemistry 275: 11075–11081. PMID: 10753912

46. Wittig I, Meyer B, Heide H, Steger M, Bleier L, et al. (2010) Assembly and oligomerization of human ATP synthase lacking mitochondrial subunits a and A6L. Biochim Biophys Acta 1797: 1004–1011. doi: 10.1016/j.bbabio.2010.02.021 PMID: 20188060

47. Stock D, Leslie AG, Walker JE (1999) Molecular architecture of the rotary motor in ATP synthase. Science 286: 1700–1705. PMID: 10576729

48. Strauss M, Hofhaus G, Schroder RR, Kuhlbrandt W (2008) Dimer ribbons of ATP synthase shape the inner mitochondrial membrane. EMBO J 27: 1154–1160. doi: 10.1038/emboj.2008.35 PMID: 18323778

49. Arnold I, Pfeiffer K, Neupert W, Stuart RA, Schagger H (1998) Yeast mitochondrial F1F0-ATP synthase exists as a dimer: identification of three dimer-specific subunits. EMBO J 17: 7170–7178. PMID: 9857174

50. Burger G, Lang BF, Braun HP, Marx S (2003) The enigmatic mitochondrial ORF ymf39 codes for ATP synthase chain b. Nucleic Acids Res 31: 2353–2360. PMID: 12711680

51. Heazlewood JL, Whelan J, Millar AH (2003) The products of the mitochondrial orf25 and orfB genes are FO components in the plant F1FO ATP synthase. FEBS Lett 540: 201–205. PMID: 12681508

52. Miranda-Astudillo H, Cano-Estrada A, Vazquez-Acevedo M, Colina-Tenorio L, Downie-Velasco A, et al. (2014) Interactions of subunits Asa2, Asa4 and Asa7 in the peripheral stalk of the mitochondrial ATP synthase of the chlorophycean alga Polytomella sp. Biochim Biophys Acta 1837: 1–13. doi: 10.1016/j.bbabio.2013.08.001 PMID: 23933283

53. van Lis R, Mendoza-Hernandez G, Groth G, Atteia A (2007) New insights into the unique structure of the F0F1-ATP synthase from the chlamydomonad algae Polytomella sp. and Chlamydomonas reinhardtii. Plant Physiol 144: 1190–1199. PMID: 17468226

54. Chevallet M, Lescuyer P, Diemer H, van Dorsselaer A, Leize-Wagner E, et al. (2006) Alterations of the mitochondrial proteome caused by the absence of mitochondrial DNA: A proteomic view. Electrophoresis 27: 1574–1583. PMID: 16548050

55. Orian JM, Hadikusumo RG, Marzuki S, Linnane AW (1984) Biogenesis of mitochondria: defective yeast H+-ATPase assembled in the absence of mitochondrial protein synthesis is membrane associated. J Bioenerg Biomembr 16: 561–581. PMID: 6242247

56. Paul MF, Velours J, Arselin de Chateaubodeau G, Aigle M, Guerin B (1989) The role of subunit 4, a nuclear-encoded protein of the F0 sector of yeast mitochondrial ATP synthase, in the assembly of the whole complex. Eur J Biochem 185: 163–171. PMID: 2553400

57. Rak M, Gokova S, Tzagoloff A (2011) Modular assembly of yeast mitochondrial ATP synthase. EMBO J 30: 920–930. doi: 10.1038/emboj.2010.364 PMID: 21266956

58. Chen C, Ko Y, Delannoy M, Ludtke SJ, Chiu W, et al. (2004) Mitochondrial ATP synthasome: three-dimensional structure by electron microscopy of the ATP synthase in complex formation with carriers for Pi and ADP/ATP. J Biol Chem 279: 31761–31768. PMID: 15166242

59. Alibu VP, Storm L, Haile S, Clayton C, Horn D (2005) A doubly inducible system for RNA interference and rapid RNAi plasmid construction in Trypanosoma brucei. Mol Biochem Parasitol 139: 75–82. PMID: 15610821

60. Wickstead B, Ersfeld K, Gull K (2002) Targeting of a tetracycline-inducible expression system to the transcriptionally silent minichromosomes of Trypanosoma brucei. Mol Biochem Parasitol 125: 211–216. PMID: 12467990

61. Surve S, Heestand M, Panicucci B, Schnaufer A, Parsons M (2012) Enigmatic presence of mitochondrial complex I in Trypanosoma brucei bloodstream forms. Eukaryot Cell 11: 183–193. doi: 10.1128/EC.05282-11 PMID: 22158713

62. Borst P, Fase-Fowler F, Gibson WC (1987) Kinetoplast DNA of Trypanosoma evansi. Mol Biochem Parasitol 23: 31–38. PMID: 3033499

63. Wirtz E, Leal S, Ochatt C, Cross GA (1999) A tightly regulated inducible expression system for conditional gene knock-outs and dominant-negative genetics in Trypanosoma brucei. Mol Biochem Parasitol 99: 89–101. PMID: 10215027

64. Oeffinger M, Wei KE, Rogers R, DeGrasse JA, Chait BT, et al. (2007) Comprehensive analysis of diverse ribonucleoprotein complexes. Nat Methods 4: 951–956. PMID: 17922018

65. Panigrahi AK, Ogata Y, Zikova A, Anupama A, Dalley RA, et al. (2009) A comprehensive analysis of Trypanosoma brucei mitochondrial proteome. Proteomics 9: 434–450. doi: 10.1002/pmic.200800477 PMID: 19105172

66. Panigrahi AK, Zikova A, Dalley RA, Acestor N, Ogata Y, et al. (2008) Mitochondrial complexes in Trypanosoma brucei: a novel complex and a unique oxidoreductase complex. Mol Cell Proteomics 7: 534–545. PMID: 18073385

67. Singha UK, Peprah E, Williams S, Walker R, Saha L, et al. (2008) Characterization of the mitochondrial inner membrane protein translocator Tim17 from Trypanosoma brucei. Mol Biochem Parasitol 159: 30–43. doi: 10.1016/j.molbiopara.2008.01.003 PMID: 18325611

68. Vondruskova E, van den Burg J, Zikova A, Ernst NL, Stuart K, et al. (2005) RNA interference analyses suggest a transcript-specific regulatory role for mitochondrial RNA-binding proteins MRP1 and MRP2 in RNA editing and other RNA processing in Trypanosoma brucei. J Biol Chem 280: 2429–2438. PMID: 15504736

69. Hannaert V, Albert MA, Rigden DJ, da Silva Giotto MT, Thiemann O, et al. (2003) Kinetic characterization, structure modelling studies and crystallization of Trypanosoma brucei enolase. Eur J Biochem 270: 3205–3213. PMID: 12869196

70. Law RH, Manon S, Devenish RJ, Nagley P (1995) ATP synthase from Saccharomyces cerevisiae. Methods Enzymol 260: 133–163. PMID: 8592441

71. Wittig I, Karas M, Schagger H (2007) High resolution clear native electrophoresis for in-gel functional assays and fluorescence studies of membrane protein complexes. Mol Cell Proteomics 6: 1215–1225. PMID: 17426019

72. Acestor N, Zikova A, Dalley RA, Anupama A, Panigrahi AP, et al. (2011) Trypanosoma brucei Mitochondrial Respiratome: Composition and organization in procyclic form. Molecular Cell Proteomics resubmitted.

73. Acestor N, Panigrahi AK, Ogata Y, Anupama A, Stuart KD (2009) Protein composition of Trypanosoma brucei mitochondrial membranes. Proteomics 9: 5497–5508. doi: 10.1002/pmic.200900354 PMID: 19834910

74. Mayhew TM, Lucocq JM (2008) Quantifying immunogold labelling patterns of cellular compartments when they comprise mixtures of membranes (surface-occupying) and organelles (volume-occupying). Histochem Cell Biol 129: 367–378. doi: 10.1007/s00418-007-0375-6 PMID: 18180944